Journal of Structural Geology 33 (2011) 220–243

Contents lists available at ScienceDirect

Journal of Structural Geology

journal homepage: www.elsevier.com/locate/jsg

Microfabrics as energy minimisers: Rotation recrystallisation as an example

Alison Ord [a,*], Bruce Hobbs [a,b]

[a] School of Earth and Environment, The University of Western Australia, 35 Stirling Highway, Crawley, Perth, Western Australia 6009, Australia
[b] CSIRO Earth Science and Resource Engineering, PO Box 1130, Bentley, Western Australia 6120, Australia

ARTICLE INFO

Article history:
Received 14 May 2010
Received in revised form
18 October 2010
Accepted 1 November 2010
Available online 24 November 2010

Keywords:
Fractals
Energy minimisation
Microstructure
Microfabric
Rotation recrystallisation
Deformation lamellae

ABSTRACT

Microfabrics are discussed as features that minimise Helmholtz energy in a system undergoing deformation and metamorphism. The energy minimisation process leads to inhomogeneous deformations and hence the formation of microfabrics at a number of scales. This process together with the requirement for compatibility both with the imposed deformation and local gradients in deformation means the microfabric must refine on smaller and smaller scales in a self-similar manner leading to fractal geometries. Nine independent levels of refinement are necessary to match the nine independent components of a general imposed deformation gradient. The process of rotation recrystallisation is proposed as one example of self similar refinement so that crystallographic preferred orientations (CPO) associated with rotation recrystallisation are presented as fractals whose fractal dimensions reflect the conditions of deformation. Compatibility also has implications for the formation of other microstructures such as non-rational deformation lamellae. The evolution and orientations of microfabrics that minimise energy are related to the history of the imposed deformation gradient (as was originally proposed by Sander) and not the strain tensor as is commonly assumed. As examples, possible models for CPO development in deformed quartz aggregates by rotation recrystallisation and the development of deformation lamellae in deformed quartz grains are presented.

1. Introduction

The hallmark of deformed metamorphic rocks is heterogeneity in the distribution of deformation. At the electron microscope scale this heterogeneity is expressed in the distribution of dislocations (McLaren et al., 1970; White, 1973; Twiss, 1976) defining lamellar structures and subgrain boundaries. At the grain scale one observes deformation and Böhm lamellae that can correspond to rational or non-rational crystallographic planes (Fairbairn, 1949; Twiss, 1974, 1976), and subgrain boundaries of various rational and non-rational orientations (Trepied et al., 1980). At the optical microscope scale, one sees domains of grains of like orientation (Sander, 1970; Hobbs, 1966; Pauli et al., 1996; Heilbronner and Tullis, 2006; although the orientations of grains within these domains can vary considerably if the complete crystallography is established: Halfpenny et al., 2006; Stipp and Kunze, 2008; Jiang et al., 2000; Bestmann and Prior, 2003) and porphyroblasts, lineations and foliations defined by variations in mineralogical composition and micro-folds. At larger scales, chevron folds, rounded folds, mineral lineations and so on are ubiquitous. Heterogeneity is developed at all scales and has been emphasised in a vast number of papers over the past 100 years (for example, Sander, 1911, 1970; Turner and Weiss, 1963; Hobbs, 1966; Oertel, 1983; Cobbold and Gapais, 1986; Gapais and Cobbold, 1987; Pauli et al., 1996; Menegon et al., 2008; Lloyd et al., 2010). The aim of this paper is to present a basis for such heterogeneity based on the formation of domainal structures as minimisers of Helmholtz energy. In addition there is a requirement that the heterogeneous deformation must be compatible from one part of the aggregate to another and also with the imposed deformation (as defined by the instantaneous deformation gradient). We show that this means fractal geometries can develop.

The observation in deformed rocks of ubiquitous unstable deformation modes as represented by inhomogeneous deformations contrasts with parallel developments in continuum mechanics that concentrated on the *stability* of deformation and hence the development of *homogeneous* deformations. This stability of deformation arises from the *Drucker postulate* (Houlsby and Puzrin, 2006, p. 31) that the Helmholtz energy of deformation is convex. We will worry later on in this paper what this statement actually means. In the early 1970's and onwards (Ericksen, 1975) people who were concerned with martensitic transformations realised that convexity of the Helmholtz energy did not explain the heterogeneity of deformation that they observed and they developed various approaches to the subject based on non-convexity of the Helmholtz

* Corresponding author.
E-mail address: alison.ord@uwa.edu.au (A. Ord).

0191-8141/$ – see front matter © 2010 Elsevier Ltd. All rights reserved.
doi:10.1016/j.jsg.2010.11.009

energy but within a framework of finite non-linear elasticity (Ericksen, 1975; Ball and James, 1987; Truskinovsky and Zanzotto, 1996). The fact that this theoretical base was involved with elastic deformations seemed to remove it from any application to plastic deformations or to the development of fractures. This approach has recently been extended to both the plastic deformation of materials and fracture development with the realisation that heterogeneity of deformation commonly observed in such materials can be approached from the same point of view as was developed for finite non-linear elasticity (for plastic deformation: Ortiz and Repetto, 1999; Carstensen et al., 2002; Miehe et al., 2004; for fracture: Francfort and Marigo, 1998; Choksi et al., 1999; Del Piero and Truskinovsky, 2001).The application of these concepts to the formation of microfabrics in deformed rocks forms the subject of this paper. The aim of this paper is to outline the general theory of heterogeneous deformation based on the above principles and then to present two possible examples namely deformation lamellae in quartz and quartz CPO development by rotation recrystallisation.

The deformation and metamorphism of rocks involves the development of fabrics at various scales. The term *fabric* is used in the sense of Turner and Weiss (1963) to mean the internal ordering of both geometrical and physical spatial data in a deformed rock; the term *microfabric* refers to the micro-scale. Vernon (2004) divides the term microfabric into *microstructure* comprising the spatial arrangements and relationships of microfabric elements such as grains, grain boundaries and foliation planes, and *preferred orientation* referring to the spatial orientations of microfabric elements including grains, domain boundaries and of crystallographic features. This paper is involved only with fabrics developed at the micro-scale and so involves length scales ranging from a few microns up to about a metre. The principles discussed here are applicable at all scales but it simplifies the discussion to concentrate on the micro-scale where for geological strain-rates the deformation can be considered isothermal (Hobbs et al., 2010, Hobbs et al., in press). As such the structures we are talking about are subgrain and grain boundaries and their geometry, the distribution of various mineral phases within the rock, the size distributions of grains and subgrains and their shapes and crystallographic preferred orientations (CPO). The distribution of mineral phases involves a huge range of microstructures including the geometries of schistosity, gneissosity, mineral lineations, porphyroblasts and various forms of metamorphic differentiation. Our concern in this paper is to develop an integrated approach to microfabric development that explains the various relations and geometries that we observe in deformed metamorphic rocks and provides a framework for relating such geometries to the conditions under which the microfabrics formed.

In some instances, microstructures have been described as fractal. Examples are sutured grain boundaries associated with recrystallisation (Kruhl and Nega, 1996), subgrain size (Streitenberger et al., 1995; Hähner et al., 1998) and grain shape (Mamtani, 2010). The fractal characteristics of these microstructures have been used to indicate temperature and strain-rate (Kruhl and Nega, 1996; Takahashi et al., 1998; Mamtani, 2010; Mamtani and Greiling, 2010). One question we seek to answer in this paper is: *Why do fractal geometries exist and what is the control on the fractal dimension that is responsible for temperature and strain-rate dependence?* The answer lies in the development of microstructures as minimisers of the Helmholtz energy of the system together with the necessity for compatibility with the imposed and local deformation gradients in order to minimise long range stresses. A second question is: *Are there other common microfabrics that have a fractal geometry and what is the significance of this fractal geometry?* One answer here concerns CPO development, especially by rotation recrystallisation. We show that such CPO patterns are fractal in nature and suggest that the fractal dimension is a measure of a range of parameters including amount of strain, temperature and strain-rate. In order to develop this approach it turns out that the important feature controlling the development at a particular instant of all of these microfabrics is the *deformation*, as measured by the *deformation gradient* and not the *strain* as is the current dominant paradigm. This means that there is a class of structures in deformed rocks that, integrated over the deformation history, is related to the kinematics of deformation rather than the resultant strain.

The structure of the paper is as follows: In Section 2 we consider the development of microfabrics as minimisers of Helmholtz energy. Section 3 considers the conditions for a given microstructure to be compatible with the imposed deformation; this condition together with minimisation of Helmholtz energy leads to fractal geometries. Section 4 discusses processes that lead to rotation recrystallisation and the related grain microstructures and fractal geometry. The discussion in Section 5 synthesises these developments and emphasises the role of kinematics in controlling the development and orientation of these structures rather than the strain. Finally in Section 6 we offer some concluding statements and point to future developments.

1.1. Notation

Symbols are defined in Table 1 and when introduced in the text. Table 2 summarises the vector/tensor/dyad notation which follows Rice (1971) and Asaro (1983). Bold faced symbols denote tensors, vectors or dyads. The magnitude of a quantity **A** is written A. Subscripts pertaining to crystal slip systems are written using Greek letters. Thus $\boldsymbol{m}_\alpha$ is a vector parallel to the normal to the slip plane, α, and $\boldsymbol{s}_\beta$ is a vector parallel to the slip direction, β. Use is made of the dyadic product in parts of this paper. The dyadic product of two vectors $\boldsymbol{a}$ and $\boldsymbol{b}$ is written $\boldsymbol{a} \otimes \boldsymbol{b}$. For excellent discussions of the dyadic product and its use in describing deformations see Nadai (1950) and Bhattacharya (2003). The Einstein summation convention is used throughout; for a discussion see Nye (1957) and Oertel (1996).

2. Microfabrics as minimisers of Helmholtz energy

Considerable progress has been made in the past 40 years in understanding the development of microstructures in the theory of finite deformation of non-linear elastic materials (Ericksen, 1975, 1998; Ball, 1977, 2004; Marsden and Hughes, 1983; Ball and James, 1987; Silhavy, 1997; Bhattacharya, 2003). As indicated in the Introduction much of this material is now known to be applicable to plastic (dissipative) deformations as well as to non-linear elastic materials (Miehe et al., 2004). The basis for the mathematical theory depends on the relationship between the stored elastic energy, Ψ, and the deformation gradient, $\boldsymbol{F}$ (Bhattacharya, 2003; relabelled the position gradient by Means, 1983; see Zhang and Hynes, 1995), defined by:

$$\boldsymbol{F} \equiv F_{ij} = \begin{bmatrix} \frac{\partial x_1}{\partial X_1} & \frac{\partial x_1}{\partial X_2} & \frac{\partial x_1}{\partial X_3} \\ \frac{\partial x_2}{\partial X_1} & \frac{\partial x_2}{\partial X_2} & \frac{\partial x_2}{\partial X_3} \\ \frac{\partial x_3}{\partial X_1} & \frac{\partial x_3}{\partial X_2} & \frac{\partial x_3}{\partial X_3} \end{bmatrix} \tag{1}$$

In (1), x_1, x_2, x_3 are the Cartesian coordinates of a material point in the current, deformed state and X_1, X_2, X_3 are the coordinates of this same point in some convenient reference state as shown in Fig. 1. Notice that for a general deformation the deformation gradient is not symmetric, so that $(\partial x_i/\partial X_j) \neq (\partial x_j/\partial X_i)(i \neq j)$, and $\boldsymbol{F}$ has 9 independent components instead of the six independent components

Table 1
List of symbols.

Symbol	Definition
a	Crystallographic **a**-axis in quartz
$\boldsymbol{a}$	Arbitrary vector
e	Internal energy
c	Crystallographic **c**-axis in quartz
$\boldsymbol{c}$	A constant vector
d	Independent degrees of freedom
$\boldsymbol{F}$, F_{ij}	Deformation gradient
$\boldsymbol{F}^{+}$, $\boldsymbol{F}^{-}$	Deformation gradients on (+) and (−) sides of a boundary
$\overline{\boldsymbol{F}}$	Mean imposed deformation gradient
f	Fractal dimension
g	Critical resolved shear stress
$\boldsymbol{I}$	Identity matrix
J	The determinant of $\boldsymbol{F}$
$\boldsymbol{l}$	A line
$\boldsymbol{Q}$	Finite rotation matrix
$\boldsymbol{m}$	Vector normal to a slip plane
$\boldsymbol{m}^{\pm}$	Vectors normal to a slip plane on the (+) and (−) sides of a boundary
$\boldsymbol{m}_{\alpha}$	Vector normal to the slip plane α
$\overline{\boldsymbol{m}}$	Effective normal to boundary between domains in a sequential laminate
$\boldsymbol{N}$	Unit normal to an interface
n	Order of a tree
n_l, n_i	Number of leaves, number of internal nodes of a tree
$\boldsymbol{R}$	Rotation matrix associated with a deformation gradient
$\boldsymbol{R}^{\pm}$	Rotation matrices associated with deformation gradients in (+) and (−) domains
r	Rank of a tree
S	Specific entropy, J kg^{-1}
$\boldsymbol{s}$	Vector parallel to a slip plane
$\boldsymbol{s}^{\pm}$	Vectors parallel to slip planes in (+) and (−) domains
$\boldsymbol{s}_{\beta}$	Vector parallel to the slip direction β
$\overline{\boldsymbol{s}}$	Effective slip direction
T	Absolute temperature, K
$\boldsymbol{U}$	Finite stretch tensor
u	A parameter
$\boldsymbol{X}$, X_i	Coordinates of a point in the undeformed state
$\boldsymbol{x}$, x_i	Coordinates of a point in the deformed state
α	Angle of rotation
α^{+},α^{-}	Relative volume proportions of laminates (+) and (−)
γ	Shear strain due to slip
$\gamma^{\pm}$	Shear strains parallel to slip planes in (+) and (−) domains
$\overline{\gamma}$	Mean shear strain
λ	Stretch
θ	An angle
ζ_r	Length scale associated with a laminate of rank r
Σ	A surface
$\boldsymbol{\sigma}$,σ_{ij}	Cauchy stress, Pa
σ_M	Maxwell stress, Pa
Ψ	Stored elastic energy; Helmholtz energy, J kg^{-1}

Table 2
Notation.

Symbol	Meaning using indices	Definition
A, **b**	A_{ij}, b_i	Second order tensor **A**, vector **b**
A, b		Magnitudes of **A** and **b**
$Q = \mathbf{A}\cdot\mathbf{B}$	$Q = A_iB_i$	Dot or scalar product of two vectors **A** and **B**
$Q = \mathbf{A}:\mathbf{B}$	$Q = A_{ij}B_{ij}$	Dot or scalar product of the two tensors **A** and **B**
$\mathbf{Q} = \mathbf{A}\cdot\mathbf{b}$	$Q_i = A_{ij}b_j$	The vector arising from the product of a second order tensor with a vector
I	I_{ij}	The identity matrix
$\mathbf{A}^{-1}$		The inverse of the matrix **A**
$\mathbf{Q} = \mathbf{m}\times\mathbf{s}$	$Q_i = \varepsilon_{ijk}m_js_k$ ε_{ijk} is the Levi-Civita or permutation symbol	Cross or vector product of two vectors **m** and **s**
$\mathbf{Q} = \mathbf{m}\otimes\mathbf{s}$	$Q_{ij} = m_is_j$	Dyadic or tensor product of the two vectors **m** and **s**
$\mathbf{A}^{T}$		Transpose of the matrix **A**

of the strain tensor. The volume change associated with the deformation is measured by J, the value of the determinant of $\boldsymbol{F}$; the deformation defined by (1) is constant-volume for $J = 1$. The significance of the deformation gradient is that it completely defines the deformation, including the stretch and rotation, of all line, surface and volume elements at each point within the body that it applies to (Bhattacharya, 2003) whereas various measures of the strain give a subset of this information; as shown in Fig. 1(b) one cannot determine the deformation given only the strain. A general deformation consists of a distortion, a rotation and a translation all three of which can vary from one point to another in the deformed body. The strain measures only the distortion. Specifically the deformation at a point $\boldsymbol{x}$ in the deformed body is given by the transformation,

$$\boldsymbol{x} = \boldsymbol{F}\boldsymbol{X} + \boldsymbol{c} \tag{2}$$

which says that each vector $\boldsymbol{X}$ in the undeformed state is distorted and rotated by the deformation gradient $\boldsymbol{F}$ and translated via a rigid motion by the vector $\boldsymbol{c}$ to become the vector $\boldsymbol{x}$. Equation (2) is referred to as a *deformation*.

The finite stretch tensor, $\boldsymbol{U}$, and the finite rotation matrix, $\boldsymbol{Q}$, are given by Bhattacharya (2003):

$$\boldsymbol{U} = \sqrt{\boldsymbol{F}^{T}\boldsymbol{F}} \text{ and } \boldsymbol{Q} = \boldsymbol{F}\boldsymbol{U}^{-1} \tag{3}$$

where the superscripts $^{\mathrm{T},-1}$ stand for the transpose and the inverse of the relevant matrix. $\boldsymbol{U}$ has the same eigenvectors as $\boldsymbol{F}^{\mathrm{T}}\boldsymbol{F}$ but the eigenvalues of $\boldsymbol{U}$ are the square roots of those of $\boldsymbol{F}^{\mathrm{T}}\boldsymbol{F}$. The deformation and strain are purely geometrical concepts that relate the reference state to the deformed state with no reference to the path of material points during the deformation. If one integrates the deformation over the path followed by material points to obtain the deformation history then one is dealing with the kinematics.

Various forms of the relationship between the Helmholtz energy and the deformation gradient are shown in Fig. 2. The definition of the Helmholtz energy as

$$\Psi = e - TS = \Psi\left(F_{ij}, T, \alpha\right) \tag{4}$$

where e is the internal energy, T is the absolute temperature and S is the entropy is well known for elastic materials (Nye, 1957) but it is perhaps not so widely appreciated that (4) is just as applicable to dissipative materials. In fact the first part of (4) written as $e = \Psi + TS$ is simply an expression of the first law of thermodynamics for a mechanical system stated as: *a quantity called the internal energy of a system exists and is made up of all the heat sources in the system*. In such a statement no distinction is drawn between heat sources arising from stored elastic energy and heat sources arising from dissipative deformations; both contribute to the internal energy. Equation (4b) contains an additional parameter, α, which is an internal variable that defines some parameter such as damage accumulation or plastic strain. The complete description of the evolution of the material involves the history of $\boldsymbol{F}$, of T and of α which commonly is also a function of $\boldsymbol{F}$ and T. Hence the evolution of Ψ with continued deformation and/or changes in temperature, depends on the history of α. Typical examples are the yielding of plastic materials (Ortiz, 1999) and the accumulation of damage (Lyakhovsky and Ben-Zion, 2008; Lyakhovsky et al., submitted for publication) where the nature of the Helmoltz energy function

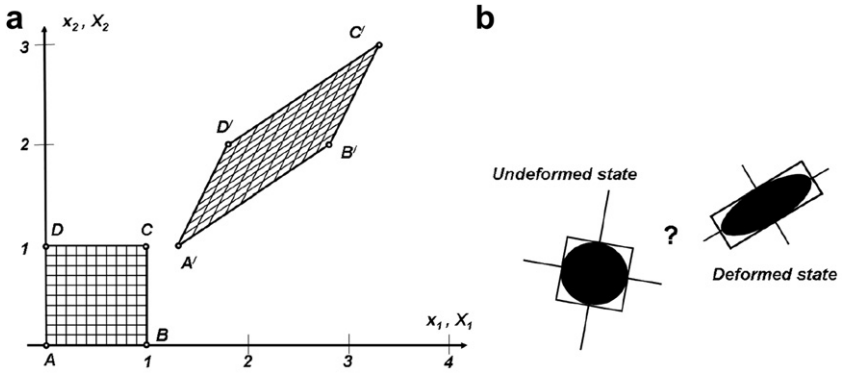

Fig. 1. The differences between a deformation and the corresponding strain. (a) The way in which the coordinates of a material point x_1, x_2, x_3 in the deformed state are related to the coordinates of this same point in some convenient reference state, X_1, X_2, X_3, defines the deformation gradient in Equation (1). The deformation, namely the complete configuration of the deformed state, including the strains, rotations and translations at each point, is defined by the deformation gradient, ***F***, as in Equation (2). The deformation for this figure is: $x_1 = 1.5X_1 + 0.5X_2 + 1.25$, $x_2 = X_1 + X_2 + 1$; the deformation is isochoric and consists of a rigid translation through a vector [1.25, 1], an anticlockwise rotation through 30.1° with principal stretches 2.065 and 0.482. (b) The strain corresponding to the deformation defined in (a). With no knowledge of the rigid rotation relative to the reference state and the rotation involved in the deformation there is no information to define the deformed shape of an initial square in the reference state; it could be a rectangle or a parallelogram. Thus the strain gives only a subset (namely the principal stretches and their orientations) of the information included in the deformation.

changes from convex to non-convex at a critical value of α. An example of a transition of this type is shown in Fig. 2(g), (h).

One of the first uses of Ψ for dissipative materials was by Biot (1955, 1958), followed by more detailed developments by Rice (1971, 1975). For a detailed discussion for both rate-dependent and rate-independent dissipative materials see Houlsby and Puzrin (1999, 2006) and for the use of the Helmholtz energy for dissipative materials in the context of this paper see in particular Miehe et al. (2002, 2004) and Hansen et al. (2010). Throughout this development, from Biot onwards, it is proposed that the behaviour of any dissipative system can be described using just two potentials, an energy (which for mechanical systems is usually most conveniently the Helmholtz energy) and the dissipation function which expresses the rate of entropy production; the dissipation function for plastic materials is the Legendre Transform of the yield surface (Houlsby and Puzrin, 1999, 2006). This development is important since it means that the stress, σ_{ij}, is related to the Helmholtz energy by $\sigma_{ij} = \rho(\partial\Psi/\partial F_{ij})$ where ρ is the density and the internal energy by $e = \sigma_{ij}F_{ij} + TS$ (for a discussion, see the above papers especially Rice, 1975, and Houlsby and Puzrin, 2006). Thus Ψ includes the energy generated by both the elastic and dissipative deformations. It is common in mechanics (Houlsby and Puzrin, 2006) to assume that Ψ is a *convex* function of the deformation gradient, ***F***. The relationship between Ψ and the strain is discussed by Pipkin (1993) and ***F*** can be replaced by some measure of the strain if this is convenient. Pragmatically, it is normal to express Ψ in terms of one of the components of ***F*** as in Figs. 2 and 6, or as some convenient measure of the strain. The mathematical treatment of this subject rapidly becomes complicated and depends heavily upon the theory of convex and non-convex functionals. We do not go down the route of mathematical rigour; the interested reader is referred to the above literature especially the papers by Ball (1977, 2004) and the book by Silhavy (1997). Ψ as a *convex* function of ***F*** is shown in Fig. 2(a). By convex here we mean the type of relation illustrated in Fig. 2(a) where the Helmholtz energy increases with some measure of the deformation gradient so as always to be convex towards the deformation gradient axis.

Since the Cauchy stress, σ_{ij}, is related to the Helmholtz energy by $\sigma_{ij} = \rho(\partial\Psi/\partial F_{ij})$, the stress–strain curve can be obtained from the Ψ–***F*** relation by differentiation. This means that a hardening stress–strain curve implies a convex form for Ψ whereas a softening stress–strain curve implies a non-convex form for Ψ. Thus the stress–strain curve corresponding to Fig. 2(a) is given in Fig. 2(b). If for instance the Ψ–***F*** relation is a quadratic as it commonly is in classical elasticity then the stress–strain curve is a straight line (dotted in Fig. 2(b)). If the Ψ–***F*** relation is of higher order than quadratic then the stress–strain curve shows increasing hardening with strain (full curve in Fig. 2(b)). A convex form of the Ψ–***F*** relation is favoured in classical continuum mechanics because it guarantees stability of the deformation so that the deformation always remains homogeneous. However we know that deformation in most materials is never stable and heterogeneities in the deformation are ubiquitous. These heterogeneities are expressed as subgrains defined by dislocation walls, deformation bands, shear zones, folds and various forms of foliations and lineations. Thus, "interesting" deformation behaviour does not arise from convex Ψ–***F*** relations which lead to homogeneous deformations and the emphasis switches to various non-convex Ψ–***F*** relations.

In order for unstable behaviour to develop, leading to microstructure formation, the Ψ–***F*** relation needs to be non-convex or else some form of bifurcation occurs (Lyakhovsky et al., 1997). In this paper we are concerned only with instabilities arising from non-convex forms of Ψ. The two important classes of non-convexity are *pseudo-convexity* (Fig. 2(c)) and *rank-1 convexity* (Fig. 2(e)). For rigorous definitions of these terms see Mangasarian (1994) and Silhavy (1997). The stress–strain curves that result from these two different Ψ–***F*** relations are shown in Fig. 2(d) and (f) respectively. These figures mean that for instabilities and hence microstructure to develop in deforming solids the response of the material to deformation must be non-linear in the ways shown in Fig. 2(d) and (f). Many experimentally deformed geological materials show stress–strain curves of this nature (for example, Heilbronner and Tullis, 2006; Delle Piane et al., 2007, 2009). For some materials, especially those that exhibit fracture, the Ψ–***F*** relation is better represented by a diagram such as Fig. 2(g) with the resultant stress–strain curve shown in Fig. 2(h) (Del Piero and Truskinovsky, 2001). Lyakhovsky and Ben-Zion (2008) have developed a thermodynamic based damage theory that leads to Ψ becoming non-convex after the accumulation of a critical level of damage. This critical level of damage would correspond to point A in Fig. 2(g).

In fluids and gases the convex relation shown in Fig. 2(a) has its analogue in the plot of Gibbs energy against the specific volume for a single phase and the stress–strain plot of Fig. 2(b) has its analogue

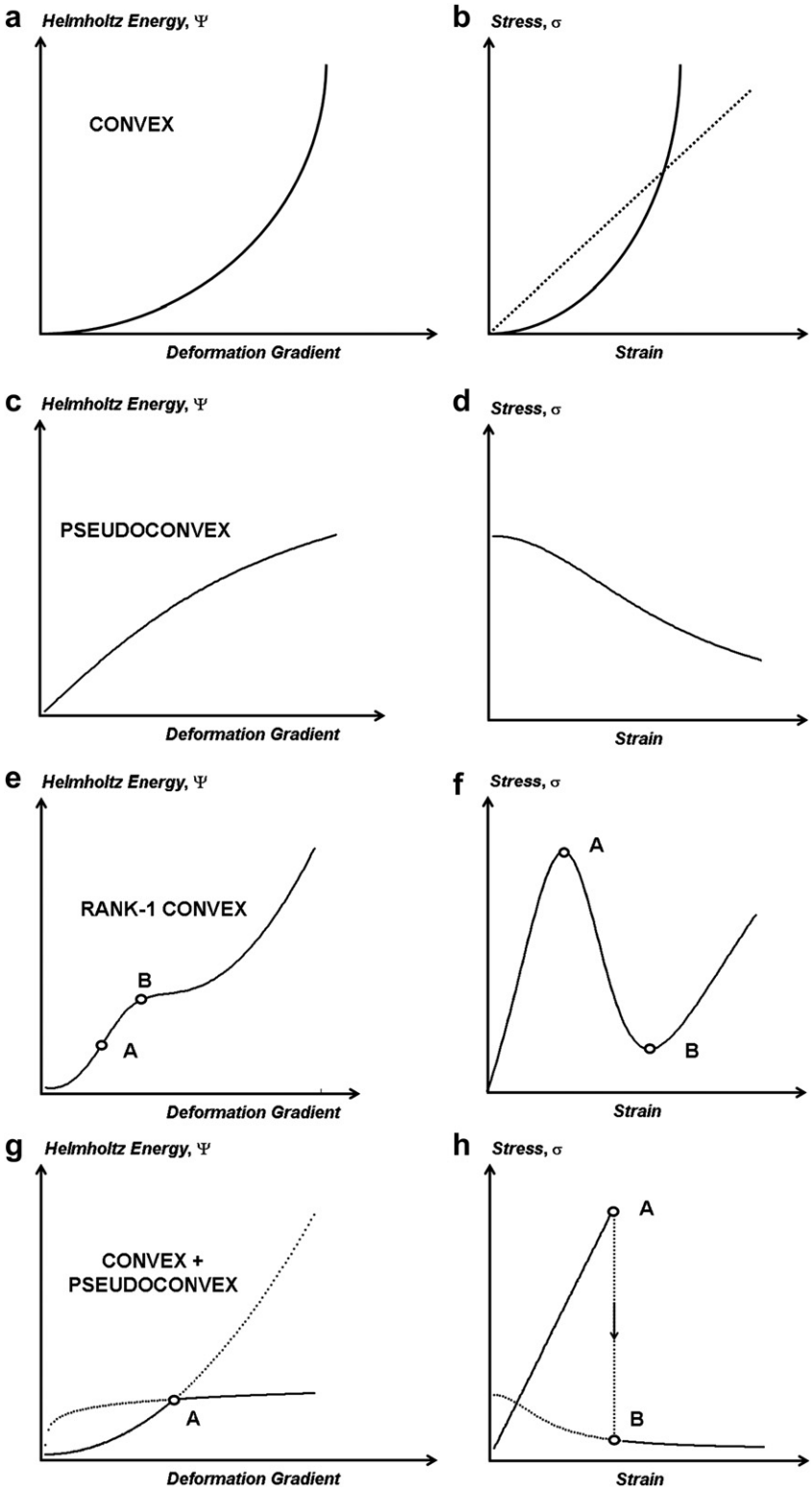

Fig. 2. Various relations between the stored energy function, Ψ, and the deformation gradient, ***F***. Also shown are the stress–strain curves corresponding to each energy function. In the diagrams in the left-hand column the measure of the deformation gradient is some convenient scalar such as F_{12}. (a) Convex Ψ–***F*** relation. (b) Stress–strain curves corresponding to (a). If the Ψ–***F*** relation in (a) is a quadratic then the stress–strain curve is linear as shown by the dotted line. If the Ψ–***F*** relation is of higher order than quadratic the stress–strain curve shows increasing hardening with strain as shown by the full curve. (c) Pseudo-convex Ψ–***F*** relation. (d) Stress–strain curve resulting from the pseudo-convex Ψ–***F*** relation in (c). (e) Rank-1 convex Ψ–***F*** relation. (f) Stress–strain curve resulting from the rank-1 convex Ψ–***F*** relation in (e). Corresponding points are marked. (g) Convex and pseudo-convex Ψ–***F*** relations combined resulting in a discontinuity at A. (h) Stress–strain curve resulting from the Ψ–***F*** relation in (g). This resembles stress–strain curves that arise from brittle behaviour with a stress drop A–B.

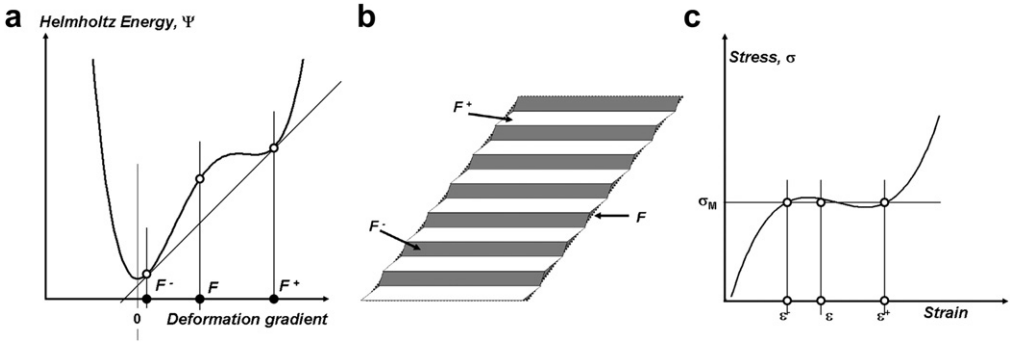

Fig. 3. Minimisation of the Helmholtz energy by the development of two sets of shear bands. (a) The Helmholtz energy is rank-1 convex and an imposed deformation gradient is represented by $\boldsymbol{F}$. The energy can be minimised by dividing the deformation into two sets of shears with deformation gradients, $\boldsymbol{F}^-$ and $\boldsymbol{F}^+$ corresponding to points where the tangent line touches the stored energy function. (b) The resulting microstructure. The imposed homogeneous deformation, $\boldsymbol{F}$, is represented by the dotted outline; the structures that minimise the energy are $\boldsymbol{F}^-$ (grey) and $\boldsymbol{F}^+$ (white). (c) The stress strain curve corresponding to the Helmholtz energy in (a). σ_M is the Maxwell stress and corresponds to that stress where the areas between the stress strain curve and the horizontal line through σ_M above and below the stress strain curve are equal. ε corresponds to the imposed strain and ε^+, ε^-, correspond to the strains in the two domains.

in the pressure-specific volume plot for a single phase (Kondepudi and Prigogine, 1998, p. 190). These kinds of relationships have been well known since the work of Gibbs (1906) and are the basis for Equilibrium Chemical Thermodynamics where the minimum in the Gibbs energy corresponds to the volume of the stable phase. The non-convexity of Fig. 2(e) has a direct analogue in Equilibrium Chemical Thermodynamics for two phase materials where the Gibbs energy becomes non-convex (Kondepudi and Prigogine, 1998, p. 193) and a tangent construction (Cahn and Larche, 1984) gives the specific volumes of the two stable coexisting phases and the pressure-specific volume plot shows a region where the pressure increases with the specific volume corresponding to a spinoidal region. In such a plot the specific volumes of the two coexisting stable phases are obtained from the Maxwell construction by equating the chemical potentials of the two phases (Kondepudi and Prigogine, 1998, p. 190).

In exactly the same way the Maxwell construction can be used for deforming systems. The tangent construction shown in Fig. 3(a) shows the way in which the Helmholtz energy of the system can be minimised for an imposed deformation gradient $\boldsymbol{F}$. Two stable deformations $\boldsymbol{F}^+$ and $\boldsymbol{F}^-$ exist and the system divides into domains corresponding to these two deformation gradients which are defined by the two points where the common tangent touches the $\Psi-\boldsymbol{F}$ curve. The resultant microstructure is shown in Fig. 3(b). The stress–strain curve corresponding to Fig. 3(a) is shown in Fig. 3(c) and σ_M is the Maxwell stress which represents the normal component of the Eshelby energy-momentum tensor (Eshelby, 1975; Silhavy, 1997) such that the area between the horizontal line through σ_M and the stress–strain curve above is equal to the area between the line and the curve below. The significance of σ_M is that it represents the stress where the stored elastic energy is sufficient to supply the energy to drive the formation of the microstructure. The stress σ_M plays the same role as the chemical potential in chemical systems (Kondepudi and Prigogine, 1998, p. 190). Similar arguments have been followed by Hunt and co-workers for the development of kink and chevron folds (Hunt et al., 2001).

2.1. What causes the Helmholtz energy to be non-convex?

Two processes associated with crystal plasticity have been identified as producing non-convex Helmholtz energy functions (Ortiz and Repetto, 1999). These processes are geometrical softening arising from single slip and latent hardening. In addition, in deforming metamorphic rocks, softening arising from chemical

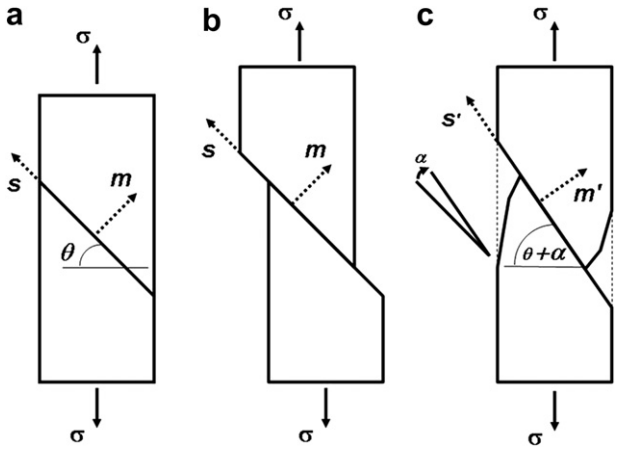

Fig. 4. Rotation of slip plane during deformation. (a) Initial geometry. $\boldsymbol{m}$ is the normal to the slip plane and $\boldsymbol{s}$ is the slip vector. σ is the extensional stress. (b) After deformation with the ends free to move. (c) After deformation with the ends constrained. $\boldsymbol{m}'$ is the new orientation of the slip plane normal and $\boldsymbol{s}'$ is the new orientation of the slip vector. The slip plane rotates through the angle α towards the extension direction.

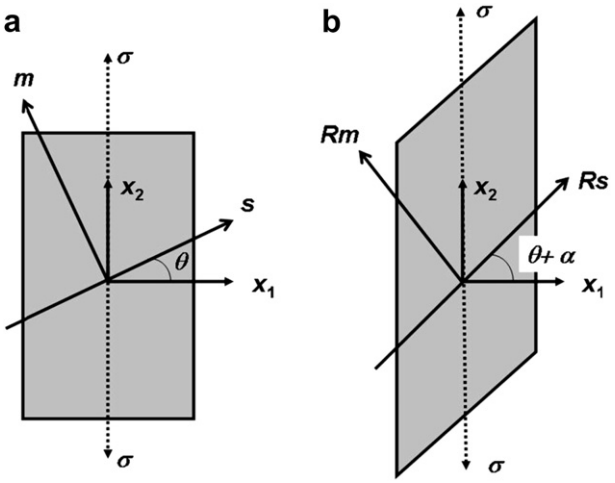

Fig. 5. Geometry of single slip deformation during extension. Vectors $\boldsymbol{m}$ and $\boldsymbol{s}$ are the slip plane normal and slip direction in the undeformed (reference) state and these become the vectors $\boldsymbol{Rm}$ and $\boldsymbol{Rs}$ in the deformed state through a rotation $\boldsymbol{R}$.

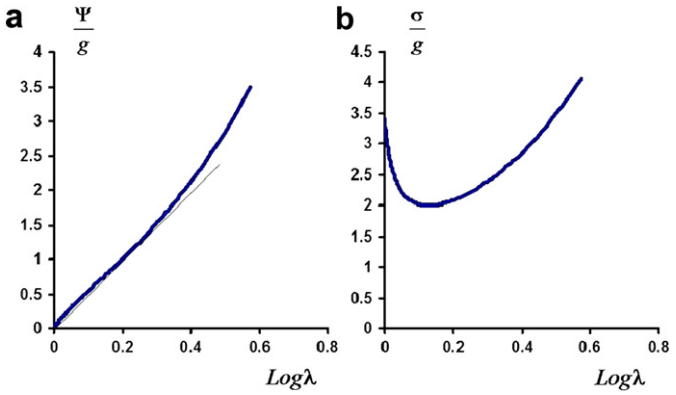

Fig. 6. Geometrical softening arising from single slip with the geometry shown in Figs. 4 and 5 with $\theta = \pi/10$. (a) Helmholtz energy plotted against the logarithm of the stretch. (b) Plastic part of the stress–strain curve derived from (a).

reactions is likely to be important. We discuss each of these mechanisms in turn below.

2.1.1. Geometrical softening

When a single crystal is deformed in extension with a single slip system operating, the slip plane tends to rotate, as shown in Fig. 4, depending on the constraints on the crystal, so that ultimately the slip plane and the slip direction align with the extension direction. Similarly, in compression, a single slip system rotates so that the normal to the slip plane tends to align with the compression axis. As the slip system rotates in the imposed deformation, geometrical softening results followed by geometrical hardening. In order to demonstrate that part of the rotation leads to geometrical softening and, more importantly, non-convex Ψ–$\boldsymbol{F}$ relations, we begin with a slip plane whose normal is $\boldsymbol{m}$ and slip direction $\boldsymbol{s}$ as shown in Fig. 4(a). The discussion follows Ortiz and Repetto (1999). The initial angle between the slip plane normal and the uniaxial extensional stress, $\boldsymbol{\sigma}$, is θ (see also Fig. 5). After deformation, if the ends are constrained, the rotation of the slip plane is α. If $\boldsymbol{R}$ is the rotation associated with the deformation then the vectors $\boldsymbol{m}$ and $\boldsymbol{s}$ become $\boldsymbol{Rm}$ and $\boldsymbol{Rs}$ after the deformation where

$$\boldsymbol{R} = \begin{bmatrix} \cos\alpha & -\sin\alpha & 0 \\ \sin\alpha & \cos\alpha & 0 \\ 0 & 0 & 1 \end{bmatrix} \text{ and } \boldsymbol{Rm} = \begin{bmatrix} -\sin(\theta+\alpha) \\ \cos(\theta+\alpha) \\ 0 \end{bmatrix},$$
$$\boldsymbol{Rs} = \begin{bmatrix} \cos(\theta+\alpha) \\ \sin(\theta+\alpha) \\ 0 \end{bmatrix} \tag{5}$$

The slip system is activated if the shear stress on the slip plane in the direction of slip is

$$\tau = \sigma\sin(\theta+\alpha)\cos(\theta+\alpha) = g \tag{6}$$

where g is the critical resolved shear stress for the slip system. The deformation gradient for crystal plasticity involving one slip system is (Rice, 1971; Asaro, 1983; Appendix B):

$$\boldsymbol{F} = \boldsymbol{R}[\boldsymbol{I} + \gamma \boldsymbol{s}\otimes\boldsymbol{m}] \tag{7a}$$

$$= \begin{bmatrix} \cos\alpha & -\sin\alpha & 0 \\ \sin\alpha & \cos\alpha & 0 \\ 0 & 0 & 1 \end{bmatrix} + \gamma \begin{bmatrix} -\cos(\theta+\alpha)\sin\theta & \cos(\theta+\alpha)\cos\theta & 0 \\ -\sin(\theta+\alpha)\sin\theta & \sin(\theta+\alpha)\cos\theta & 0 \\ 0 & 0 & 1 \end{bmatrix} \tag{7b}$$

We take $\boldsymbol{F}$ to be constrained such that there is a stretch of λ and a shear parallel to x_2 as shown in Fig. 5 and no shear parallel to x_1. This means that an initial unit vector parallel to x_2 with components [0 1 0] is acted upon by $\boldsymbol{F}$ to become the vector [0 λ 0] according to

$$\boldsymbol{F}\begin{bmatrix} 0 \\ 1 \\ 0 \end{bmatrix} = \begin{bmatrix} 0 \\ \lambda \\ 0 \end{bmatrix} \tag{7c}$$

In (7a) $\boldsymbol{I}$ is the identity matrix, γ is the shear strain due to slip and $\otimes$ denotes the dyadic product between two vectors. Use of (7b) with (6) and the relation (7c) gives

$$\sigma = \frac{g}{\sin(\theta+\alpha)\cos(\theta+\alpha)};\ \gamma = \frac{\sin\alpha}{\cos(\theta+\alpha)\cos\theta};$$
$$\lambda = \cos\alpha + \frac{\sin\alpha\sin(\theta+\alpha)}{\cos(\theta+\alpha)} \tag{8}$$

This enables us to plot the Helmholtz energy, $\Psi = g\gamma$, against log λ, as shown in Fig. 6(a) for $\theta = \pi/10$. Also shown in Fig. 6(b) is the resulting stress–strain curve.

The Ψ–$\boldsymbol{F}$ relation is non-convex between log $\lambda = 0$ and ca. 0.3 and gives rise to a softening and then a hardening $\boldsymbol{\sigma}$–$\boldsymbol{F}$ curve. Although the departure from convexity is small it is sufficient to represent a significant softening response in the stress–strain curve. As such we expect geometrical softening to give rise to microstructure in the form of alternating domains with different deformation gradients. This type of behaviour has been reported in metals (Dillamore et al., 1979; Asaro, 1983; Ortiz and Repetto, 1999). Although we have discussed geometrical softening from the point of view of crystal plasticity the same general principles hold for any material that deforms by shearing parallel to a single plane. Hence the deformation of thinly layered or foliated rocks may be expected to develop geometrical softening if the deformation approximates shearing parallel to these planes and micro-folds develop as a response to minimising Ψ (Hunt et al., 2001).

2.1.2. Latent hardening

Latent hardening refers to the hardening of one slip system due to interaction with dislocations from another slip system and is well documented in metal plasticity (Asaro, 1983; Havner, 2005). The process preferentially hardens that slip system relative to the interacting system. Piercy et al. (1955) and Kocks (1960) pointed out that such interactions inhibit the simultaneous operation of more than one slip system throughout a grain so that although five independent slip systems may perhaps operate within a grain, only one operates at each place within a grain. The result is a domainal structure within each grain where one slip system dominates within each domain. Asaro (1983) refers to such microstructure as "patchy slip". Ortiz and Repetto (1999) proceed to show that the operation of single slip within one part of a grain corresponds to a Helmholtz energy minimum so that the process of latent hardening leads to a spatial distribution of single slip that minimises the Helmholtz energy of the system. This work has been extended by Hansen et al. (2010). Although there is no experimental work on silicates that demonstrates the existence of latent hardening, one expects the process to dominate the crystal plasticity of silicates, at least over some as yet undetermined temperature-strain-rate field, as it does in metals so that domainal structures should be common, as is observed (Pauli et al., 1996; Vernon, 2004, his fig. 5.17–5.28).

2.1.3. Chemical softening

There are relatively few experiments that demonstrate the influence of mineral reactions on the mechanical properties of

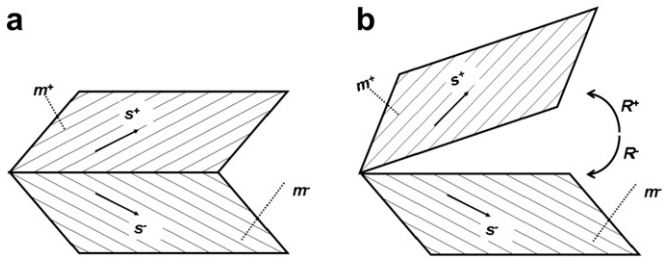

Fig. 7. Deformation in two adjacent domains. (a) Deformation on slip systems ($\boldsymbol{s}^{\pm}$, $\boldsymbol{m}^{\pm}$) in two initially adjacent domains. (b) The same result as (a) can be obtained with slip on ($\boldsymbol{s}^{\pm}$, $\boldsymbol{m}^{\pm}$) and rotations $\boldsymbol{R}^{\pm}$.

silicates (Brodie and Rutter, 1987; Stunitz and Tullis, 2001; de Ronde et al., 2004). In general these studies show a weakening effect arising from the chemical reactions and support a number of other discussions on the influence of mineral reactions on mechanical properties (Rubie, 1983; Wintsch, 1985). Such weakening is consistent with a non-convex Ψ–$\boldsymbol{F}$ relation as shown in Figs. 2 and 3 and hence microstructures are expected to form in order to minimise the Helmholtz energy. The situation is somewhat complicated in the case of chemical softening because factors other than a simple feedback between mineral reaction and deformation come into play. These include in particular the influence of grain-size reduction arising from the mineral reaction and the additional complexity of strain-rate softening (Hobbs et al., 2010).

3. Compatibility with imposed deformation and fractal microstructures

There are two aspects of deformation compatibility in an inhomogeneously deformed material. One is local compatibility between deformations in adjacent domains and the other is global compatibility of the array of deformed domains with the imposed deformation. In both instances we require the microstructure to develop with no gaps or overlaps. This requirement also eliminates any local stress concentrations and long range stresses.

The previous discussion has shown that for materials that are characterised by a non-convex Helmholtz energy potential and deformed by a deformation gradient, $\boldsymbol{F}$, the Helmholtz energy is minimised by dividing the body into two domains of differing deformation gradients, $\boldsymbol{F}^{+}$ and $\boldsymbol{F}^{-}$, but which add together, according to their volume fractions, α^{+} and α^{-}, to produce the mean imposed deformation gradient; the Helmholtz energy for such materials is not minimised by a homogeneous deformation (Bhattacharya, 2003). The mean imposed deformation gradient, $\boldsymbol{F}^{-}$, is given by

$$\overline{\boldsymbol{F}} = \alpha^{-}\boldsymbol{F}^{-} + \alpha^{+}\boldsymbol{F}^{+};\ \alpha^{-} + \alpha^{+} = 1 \tag{9}$$

This situation is illustrated in Fig. 3(b) where $\alpha^{+} \approx \alpha^{-}$. Compatibility of deformation across the interface between the two deformations requires (see Appendix A) that

$$\boldsymbol{F}^{+} - \boldsymbol{F}^{-} = \boldsymbol{a}\otimes\boldsymbol{N};\ N = 1 \tag{10}$$

$\boldsymbol{N}$ is the unit normal to the interface and $\boldsymbol{a}$ is an arbitrary vector. The condition (10) is known as rank-1 compatibility since in order for compatibility to be achieved ($\boldsymbol{F}^{+} - \boldsymbol{F}^{-}$) must constitute a rank-1 matrix (see Appendix A; Silhavy, 1991, 1997; Bhattacharya, 2003). One can show that the dyadic product of two vectors (in this case, $\boldsymbol{a}$ and $\boldsymbol{N}$) is always a rank-1 matrix. Equation (10) is a very powerful relationship and enables one to check or prescribe the conditions for compatibility across any boundary between two deformations (Appendix A).

Moreover, if deformation within the two domains is by shear parallel to planes whose normals are $\boldsymbol{m}^{\pm}$ in directions $\boldsymbol{s}^{\pm}$ as shown in Fig. 7 then the deformation gradient in each domain consists of rotations $\boldsymbol{R}^{\pm}$ together with shears $\gamma^{\pm}\boldsymbol{s}^{\pm}\otimes\boldsymbol{m}^{\pm}$ where $\gamma^{\pm}$ are the shear strains arising from slip within the two domains respectively. These deformation gradients are expressed (Appendix B) by

$$\boldsymbol{F}^{\pm} = \boldsymbol{R}^{\pm}\left(\boldsymbol{I} + \gamma^{\pm}\boldsymbol{s}^{\pm}\otimes\boldsymbol{m}^{\pm}\right) \tag{11}$$

Equations (9), (10) and (11) mean that once $\boldsymbol{m}^{\pm}$ and $\boldsymbol{s}^{\pm}$ are prescribed, the volume proportions of the two domains are fixed by prescribing one of the α's since $\alpha^{-} + \alpha^{+} = 1$ giving one degree of freedom. In addition four possibilities exist for the domains prescribed by choices of $\boldsymbol{R}^{\pm}$ and $\gamma^{\pm}$ resulting in four rank-1 constraints of the form (10). Thus for an array of laminates of the form shown in Fig. 7 there is one degree of freedom (α^{+} or α^{-}) and four constraints.

However the development of these two deformation gradients cannot fully match the imposed deformation and gaps always remain as shown in Fig. 3(b) with the implication that long range stresses remain so that the Helmholtz energy is not fully minimised. One way of overcoming this situation is to produce the two deformations on a finer scale as shown in Fig. 8. Gaps still remain and the next stage in minimising the Helmholtz energy is to produce fine scale structure within the gaps (Ball and James, 1987, their Fig. 6). An example is shown in Fig. 9(c), (d) where self similar refinement of the broad scale kinking comprised of simply $\boldsymbol{F}^{+}$ and $\boldsymbol{F}^{-}$ is illustrated. This refinement process is referred to as sequential lamination by various authors including Kohn (1991) and Ortiz and Repetto (1999) and we follow their approach below.

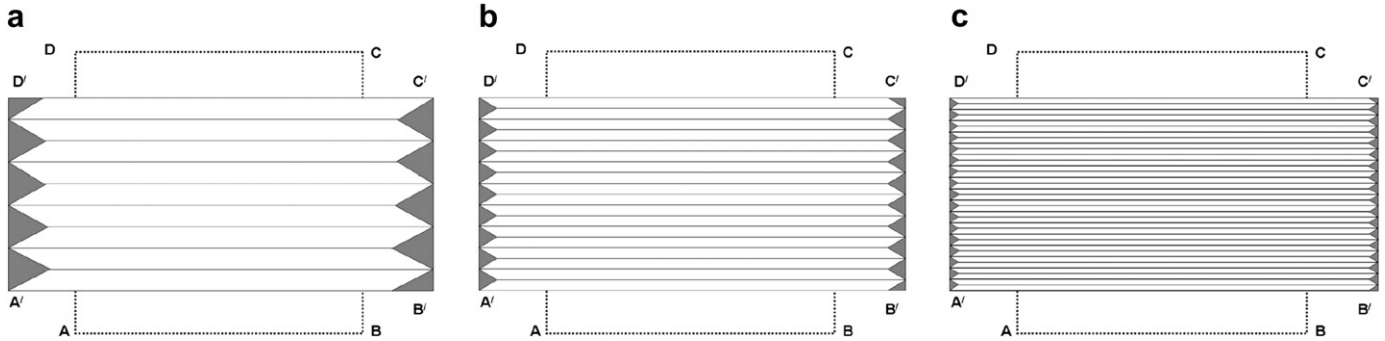

Fig. 8. The square ABCD is deformed to become the rectangle A/B/C/D/. The deformation is approximated by alternating sheared zones with equal thicknesses but opposite senses of shear. As the thickness of the sheared zones is decreased the inhomogeneous deformation field comes closer to approximating the imposed homogeneous deformation. The error in matching (denoted by the grey areas) becomes smaller with the decrease in thickness and in this case is proportional to the thickness of the individual sheared zones.

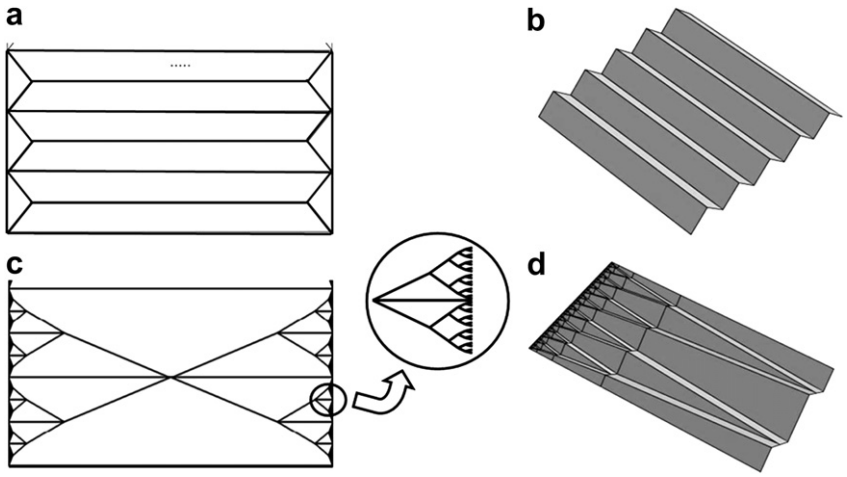

Fig. 9. Self-similar refinement of a microstructure to attempt to match an imposed deformation. (a) Coarse microstructure with gaps represented in three dimensions in (b). (c) Self similar refinement of the microstructure to fit the imposed deformation. (d) Three dimensional arrangement of the self-similar microstructure. (Adapted from M. Ortiz, Presentation at the International Congress of Theoretical and Applied Mechanics, Adelaide, Australia, 2008).

In order to describe this refinement process and to understand how it leads to compatibility with the imposed deformation gradient it is convenient to classify the various levels of refinement according to their *rank*. The homogeneous imposed deformation gradient is referred to as *rank 0* and is represented by the deformed rectangle $A'B'C'D'$ in Fig. 8 or the deformed parallelogram representing $\boldsymbol{F}$ in Fig. 3(b). Laminates (or domains) of *rank 1* are the next level of refinement such as $\boldsymbol{F}^+$ and $\boldsymbol{F}^-$ in these figures. A laminate of *rank r* is a mixture of two *rank (r-1)* laminates. Kohn (1991) points out that there is a length scale, ζ_r, associated with each rank such that $\zeta_r > \zeta_{r-1}$. Kohn also speculates on the development of sequential refinement structures not comprised of laminar regions (which we have called "laminates" here following Ortiz and Repetto, 1999) but of other shapes. To date there is no mathematical treatment of such possibilities. The stacking of various domains to approximate an imposed deformation was discussed and illustrated in an insightful manner by Turner and Weiss (1963, pp. 366–382) and perhaps it is geologically more relevant in some instances (especially recrystallisation microstructures) to think of the "laminates" in terms of these other (more equant) microstructural arrangements. We return to this possibility in Section 4.

It is convenient to think of the sequential refinement process in terms of a binary tree structure as shown in Fig. 10(a). The tree is composed of a number, n, of nodes arranged in levels. The number of levels is the rank, r, of the tree. n is the order of the tree. Each node is occupied by a deformation gradient $\boldsymbol{F}_i$, $i = 1,\ldots n$. The imposed homogeneous deformation is $\boldsymbol{F}_1$ and corresponds to level 0. Each node has either two *children* or none. Nodes with a common parent are called *siblings* and nodes with no children are called *leaves*. Nodes that are not leaves are called *internal nodes*. The deformation gradient associated with children of node i are denoted as $\boldsymbol{F}_i^{\pm}$. Each level, l, therefore contains at most 2^l nodes. An example is illustrated in Fig. 10 and represents a rank-3 laminate with order 11. The leaves of the tree are nodes 6–11. Nodes 4 and 5 in level 2 correspond to deformation gradients $\boldsymbol{F}_2^- = \boldsymbol{F}_4$ and $\boldsymbol{F}_2^+ = \boldsymbol{F}_5$. The structure of the sequential laminate corresponding to this tree is shown in Fig. 10(b).

We now consider what is required for a self-similar sequential laminate to achieve compatibility with an imposed deformation gradient. The assumption is that the deformation within each laminate is achieved solely by isochoric shear parallel to a single plane. Then the deformation gradient associated with a leaf i is $\boldsymbol{F}_i = \boldsymbol{R}_i(\boldsymbol{I} + \gamma_i \boldsymbol{s}_i \otimes \boldsymbol{m}_i)$ so that such a deformation introduces four degrees

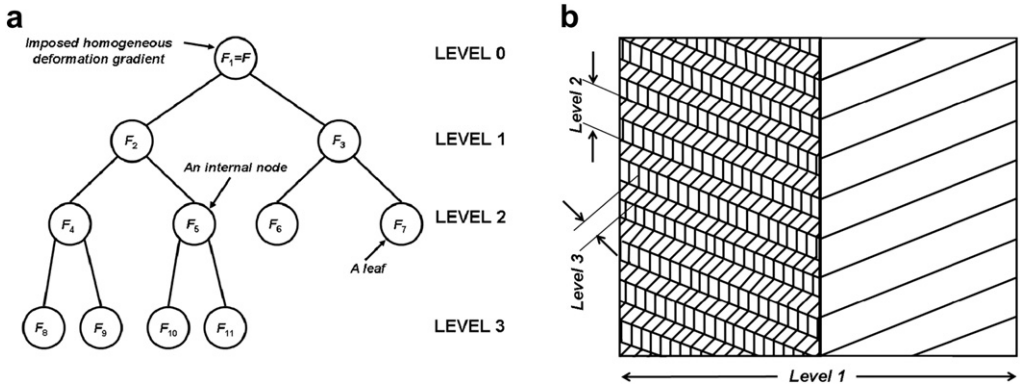

Fig. 10. The multi-level structure corresponding to the sequential refinement process that produces compatibility of the deformations within a sequential laminate system with an imposed deformation. (a) The tree structure for a rank-3 laminate with order 11. (b) The corresponding microstructure. Adapted from Ortiz and Repetto (1999).

of freedom $(\pm)\boldsymbol{R}_i$ and $(\pm)\gamma_i$. We have seen above that an internal node involves one independent degree of freedom and four constraints. Thus the number of independent degrees of freedom, d, for the system is

$$d = 4n_l - 3n_i \tag{12}$$

where n_l and n_i are the numbers of leaves and internal nodes respectively. In order to produce compatibility with the imposed deformation gradient, nine independent degrees of freedom are required so that $d \geq 9$. This cannot be achieved with a rank-1 laminate where $n_l = 2$ and $n_i = 1$ where $d = 5$. For the system shown in Fig. 10, $n_l = 6$ and $n_i = 5$ so that $d = 9$. The required number of degrees of freedom cannot be achieved with two complete levels so that at a minimum, three levels are required to produce compatibility.

The self-similar refinement shown in Fig. 9 is identical to the self-similar refinement involved in producing many fractal structures such as Cantor dust, Koch curves and various fractal trees (Mandelbrot, 1983). Thus the tree structure illustrated in Fig. 10(a) is exactly that required for a dyadic Cantor dust fractal. Hence if one intersected the microstructure with a line one would expect to produce intersections with a fractal dimension identical to that of a Cantor dust with a fractal dimension of approximately 0.6 (Mandelbrot, 1983, p. 77). Equally, if one were to trace the boundaries between different domains in Fig. 9(c) one produces a triadic Koch curve and expects fractal dimensions somewhere in the range 1.1–1.5. Similarly if one could measure the fractal dimensions of such refining microstructures in three dimensions one expects fractal dimensions resembling those of Menger sponges with fractal dimensions around 2.7. There are very few measurements of the fractal dimensions of microstructures but those of Kruhl and Nega (1996) obtain fractal dimensions between 1.017 and 1.289 for sutured grain boundaries in quartz and point out the resemblance to Koch curves. We return to this issue in Section 5. Examples of self-similar refining microstructures are shown by Vernon (2004, his fig. 4.50 in a microcline perthite) and in a spectacular manner by Hull (1999) for microfractures.

4. Examples: deformation lamellae and crystallographic preferred orientations in quartz aggregates

Although crystallographic preferred orientations (CPO's) of quartz had been extensively studied since the pioneering work of Sander (1911, 1930) it was not until the papers by Lister et al. (1978) and Lister and Hobbs (1980) that a rigorous theoretical framework for explaining the development of CPO's and their relationship to the kinematics of deformation was proposed. These papers also set the scene for interpretation of quartz CPO's in terms of amount of strain, temperature and strain-rate. The theory rests on the work of Taylor (1938) and Bishop and Hill (1951) and depends on the existence of five independent slip systems (Paterson, 1969) to produce compatibility with the imposed boundary conditions of a homogeneous incremental strain at each instant during the deformation history. It also assumes that the strain in each grain is homogeneous and identical to the imposed strain and that the only mechanism of deformation is crystal slip.

The Taylor-Bishop-Hill approach is amazingly successful and comes very close to duplicating experimentally produced CPO's in metals (Bronkhorst et al., 1992; Miehe et al., 2002) for plane strain and triaxial shortening and simple shearing deformation histories. This is somewhat surprising because the deformation of individual grains is rarely homogeneous and the strain from one grain to the next is variable depending on the crystallographic orientation relative to the imposed deformation. Moreover in some minerals it is not clear that five independent slip systems are operative or even available. In order to make up five independent slip systems in quartz the $\langle \mathbf{c} \pm \mathbf{a} \rangle$ Burgers vectors are required along with $\langle \mathbf{a} \rangle$ and $[\mathbf{c}]$. Although the $\langle \mathbf{c} \pm \mathbf{a} \rangle$ Burgers vectors have been identified using the invisibility criterion with transmission electron diffraction (Ord and Kirby, 1982; Trepied and Doukhan, 1982) its operation is much more difficult than the operation of the $\langle \mathbf{a} \rangle$ and $[\mathbf{c}]$ Burgers vectors (Linker et al., 1984). Following the observations of Schmid and Casey (1986) the tendency in the literature is to describe the development of a particular CPO as the operation of just one slip system such as "basal-$\langle \mathbf{a} \rangle$" or "prism-$[\mathbf{c}]$". In some minerals such as olivine five independent slip systems do not exist and resort has been made to self-consistent methods (Tome et al., 2002; Kocks et al., 1998; Wenk, 1999). Schmid and Casey (1986) point out that the Taylor-Bishop-Hill approach fails to predict some types of quartz fabrics. The situation is made even more interesting by the observation that CPO's associated with the rotation recrystallisation mechanism are not necessarily the same as those developed in the un-recrystallised matrix (Stipp et al., 2002; Mancktelow, 2004; Jeřábek et al., 2007) although the orientations of such grains suggest that crystal plasticity by slip is operative in the rotation mechanism (Schmid and Casey, 1986; Heilbronner and Tullis, 2006). The questions that arise from this brief review are: *What is the process that makes it possible to produce CPO's in quartz with the operation of just one slip system and compatibility of deformation throughout the aggregate? And is such a process related to rotation recrystallisation?* In what follows we first review the observations on slip systems in quartz and then discuss these observations in the light of energy minimisation concepts. This leads to a discussion of rotation recrystallisation and the suggestion that quartz CPO's can be fractal.

4.1. Observed slip systems and slip features in quartz: deformation lamellae

A large number of planar structures has been described from naturally and experimentally deformed quartz based on optical and transmission electron microscope (TEM) studies and on observations of slip bands on the surfaces of single crystals whose surfaces were polished before deformation (Christie et al., 1964; Baeta and Ashbee, 1968, 1969a,b; McLaren et al., 1970; White, 1973; Ardell et al., 1974; Twiss, 1974, 1976; Morrison-Smith et al., 1976; Linker et al., 1984). Although such structures were first described by Sander (1930) and many studies followed (Fairbairn, 1949, and references therein), the group of papers mentioned above between 1964 and 1984 concentrated essentially on interpreting these structures in terms of the slip systems operating in quartz. The outcome is that these planar features are invariably expressed as some form of subgrain structure in TEM studies and invariably have non-rational crystallographic orientations although in some instances the features may be close to rational planes. Fairbairn (1949) in particular emphasises the non-rational nature of deformation lamellae and presents data showing that the angle between the **c**-axis and the pole to the lamella can vary between 0° and 80° with a concentration between about 7° and 35°. The slip planes inferred from these studies are the basal plane (0001), the first and second order prism planes $\{10\bar{1}0\}$ and $\{1\bar{2}10\}$, and the positive and negative rhombohedra $\{10\bar{1}1\}$ and $\{01\bar{1}1\}$. The determination of Burgers vectors is however much more problematic. It seems that both $\mathbf{a}$ $\langle 2\bar{1}\bar{1}0\rangle$ and $\boldsymbol{c}[0001]$ have been confirmed unambiguously using the invisibility criterion in TEM (Baeta and Ashbee, 1968; Ardell et al., 1974; Morrison-Smith et al., 1976). There are two TEM confirmations of a $\langle \mathbf{c} \pm \mathbf{a} \rangle$ Burgers vector (Ord and Kirby, 1982; Trepied and Doukhan, 1982) although many workers have proposed $\langle \mathbf{c} \pm \mathbf{a} \rangle$ as a slip direction from surface slip band observations. The $\langle \mathbf{c} \pm \mathbf{a} \rangle$ slip direction is necessary to achieve five independent slip systems in quartz. Baeta and Ashbee (1969a) suggest that perhaps the $\langle \mathbf{c} \pm \mathbf{a} \rangle$

Table 3
Slip systems in α-quartz and direction cosines for slip plane normals and slip directions.

System	m	s	Direction cosines of slip plane normal	Direction cosines of positive slip directions
Basal a	$\perp(0001)$	$\pm\langle\mathbf{a}\rangle$	(0001); [0, 0, 1]	$\mathbf{a}_1$: [1, 0, 0] $\mathbf{a}_2$: [−0.5, 0.866, 0] $\mathbf{a}_3$: [−0.5, −0.866, 0]
Prism a	$\perp\{01\bar{1}0\}$	$\pm\langle\mathbf{a}\rangle$	$m_1(01\bar{1}0)$: [0, 1, 0] $m_2(10\bar{1}0)$: [0.866, 0.5, 0] $m_3(1\bar{1}00)$: [0.866, −0.5. 0]	$\mathbf{a}_1$: [1, 0, 0] $\mathbf{a}_2$: [−0.5, 0.866, 0] $\mathbf{a}_3$: [−0.5, −0.866, 0]
Prism c	$\perp\{01\bar{1}0\}$	$\pm\mathbf{c}$	$m_1(01\bar{1}0)$: [0, 1, 0] $m_2(10\bar{1}0)$: [0.866, 0.5, 0] $m_3(1\bar{1}00)$: [0.866, −0.5. 0]	**c**: [0, 0, 1]
Rhomb a	$\perp\{0\bar{1}11\}$	$\pm\langle\mathbf{a}\rangle$	$r_1(0\bar{1}11)$: [0, −0.7857, 0.6187] $r_2(10\bar{1}1)$: [0.6803, 0.3934, 0.6187] $r_3(\bar{1}101)$: [-0.6803, 0.3934, 0.6187]	$\mathbf{a}_1$: [1, 0, 0] $\mathbf{a}_2$: [−0.5, 0.866, 0] $\mathbf{a}_3$: [−0.5, −0.866, 0]
Rhomb c+a	$\perp\{0\bar{1}11\}$	$\pm\langle\mathbf{c}+\mathbf{a}\rangle$ $\pm\langle\mathbf{c}-\mathbf{a}\rangle$	$r_1(0\bar{1}11)$: [0, −0.7857, 0.6187] $r_2(10\bar{1}1)$: [0.6803, 0.3934, 0.6187] $r_3(\bar{1}101)$: [-0.6803, 0.3934, 0.6187]	$[\mathbf{c}+\mathbf{a}_1]$: [−0.6726, 0, 0.74] $[\mathbf{c}-\mathbf{a}_1]$: [0.6726, 0, 0.74] $[\mathbf{c}+\mathbf{a}_2]$: [−0.3363, 0.5826, 0.74] $[\mathbf{c}-\mathbf{a}_2]$: [0.3363, −0.5826, 0.74] $[\mathbf{c}+\mathbf{a}_3]$: [−0.3363, −0.5826, 0.74] $[\mathbf{c}-\mathbf{a}_3]$: [0.3363, 0.5826, 0.74]

Burgers vector dissociates into ⟨**a**⟩ and **[c]** Burgers vectors but there is no evidence of stacking faults in quartz to confirm this.

Despite all this work the situation remains confused with a lack of consistent terminology (despite several efforts) and a bewildering array of observations including rational and non-rational lamellae structures and planar domains with and without lattice rotations. There is the added point to be taken into consideration, namely that many common quartz CPO's can be satisfactorily interpreted in terms of the operation of one Burgers vector (⟨**a**⟩ in the case of Schmid and Casey, 1986). In the following we apply the concepts developed by Ortiz and Repetto (1999) to try and bring a systematic approach to the observations.

4.2. Domainal structure at the slip band scale

The discussion of geometrical softening and latent hardening in Section 2 leads to the conclusion that the Helmholtz energy function associated with these processes is non-convex. Geometrical softening (and hardening) arises when one slip system operates within a part of a grain; both geometrical softening and latent hardening lead to "patchy slip" where again one slip system operates in a part of a grain. Hence we are looking for situations where single slip operates at least locally. Under such conditions a homogeneous deformation does not minimise the energy and the crystal can lower its Helmholtz energy by adopting some form of microstructure. We explore the possibility that this microstructure consists of alternating regions or domains where one slip system operates within each region but different slip systems may operate from one domain to the next. As such the problem reduces to the following: *Given an imposed deformation gradient and the array of slip systems known to operate in quartz, what kinds of lamellar or domainal structures are geometrically possible?* By geometrically possible here we mean that the deformation is compatible from one lamella or domain to another and no gaps or overlaps develop.

This problem is one of compatibility. The deformation gradient in each domain is given by $\boldsymbol{F}^{\pm}=\boldsymbol{R}^{\pm}(\boldsymbol{I}+\gamma^{\pm}\boldsymbol{s}^{\pm}\otimes\boldsymbol{m}^{\pm})$ and compatibility across the interface between domains is guaranteed for $\boldsymbol{F}^{+}-\boldsymbol{F}^{-}=\boldsymbol{a}\otimes\boldsymbol{N}$ as discussed above and in Appendices A and B. These equations enable one to calculate the complete array of possible domainal structures that can form for an imposed deformation gradient given the list of available slip systems. We leave this accounting to a future paper and instead give an idea of what is possible. One can distinguish two types of domains: *Non-degenerate domains* where different slip systems operate either side of the boundary and *degenerate domains* where some aspect of the slip system either side of the boundary (the slip direction or the slip plane normal or both) is the same and has the same orientation either side of the boundary.

We consider the slip systems for quartz summarised in Table 3. Here only those slip systems associated with the basal plane (0001), the first order prism planes $\{10\bar{1}0\}$ and the negative rhombs $\{01\bar{1}1\}$ have been included. We adopt the convention that $\boldsymbol{m}_{\alpha}$ is a unit vector parallel to the normal to the slip plane α in the positive direction of the normal and $\boldsymbol{s}_{\beta}$, $-\boldsymbol{s}_{\beta}$ are vectors parallel to the slip direction β in the positive and negative directions respectively. The coordinate conventions we adopt for α-quartz are shown in Fig. 11 and the terminology follows Linker et al. (1984, their fig. 1). With these conventions the direction cosines of the various slip systems can also be included in Table 3.

Ortiz and Repetto (1999) define two basic types of interface between two deforming crystal plastic domains. In one type (called non-degenerate interfaces) the deformation on at least one side of the boundary requires rotation, $\boldsymbol{R}^{\pm}$, in order to maintain compatibility during the progressive deformation. The other type of boundary (degenerate) requires no rotation to maintain

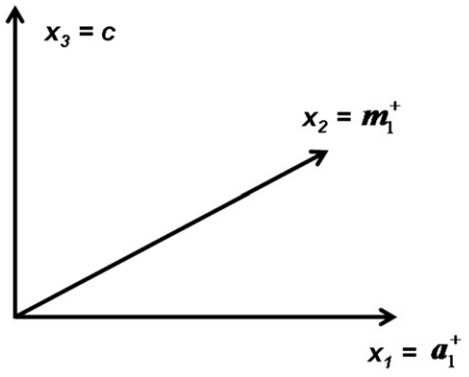

Fig. 11. Coordinate convention used for α-quartz in this paper. The terminology follows Linker et al. (1984, their fig. 1).

compatibility. These second types of boundaries can be kink, subgrain or grain boundaries.

4.2.1. Non-degenerate interfaces are defined by the requirements

$$\left[\left(\boldsymbol{R}^{+}\boldsymbol{s}^{+}\times\boldsymbol{R}^{+}\boldsymbol{m}^{+}\right)\cdot\boldsymbol{s}^{-}\right]\left[\left(\boldsymbol{R}^{+}\boldsymbol{s}^{+}\times\boldsymbol{R}^{+}\boldsymbol{m}^{+}\right)\cdot\boldsymbol{m}^{-}\right]\neq 0 \tag{13a}$$

$$\left[\left(\boldsymbol{s}^{-}\times\boldsymbol{m}^{-}\right)\cdot\boldsymbol{R}^{+}\boldsymbol{s}^{+}\right]\left[\left(\boldsymbol{s}^{-}\times\boldsymbol{m}^{-}\right)\cdot\boldsymbol{R}^{+}\boldsymbol{m}^{+}\right]\neq 0 \tag{13b}$$

Ortiz and Repetto (1999) show that at least in BCC metals the interfaces for non-degenerate domains are always rational crystallographic planes. If we look only at an infinitesimal deformation and take $\boldsymbol{R}^{+}=\boldsymbol{R}^{-}=\boldsymbol{I}$ in both the conditions (13a) and (13b) one can see that for all combinations of basal $\langle\mathbf{a}\rangle$ slip (+) and prism $\langle\mathbf{a}\rangle$ slip (−), $(\boldsymbol{s}^{+}\times\boldsymbol{m}^{+})$ is a vector parallel to [**c**] and hence $(\boldsymbol{s}^{+}\times\boldsymbol{m}^{+})\cdot\boldsymbol{s}^{-}$ is always zero. Similarly $(\boldsymbol{s}^{-}\times\boldsymbol{m}^{-})$ is parallel to $\langle\mathbf{a}\rangle$ and hence $(\boldsymbol{s}^{-}\times\boldsymbol{m}^{-})\cdot\boldsymbol{m}^{+}$ is always zero. Thus all of these laminates are degenerate. For basal $\langle\mathbf{a}\rangle$ slip (+) combined with prism [**c**] slip (−), $(\boldsymbol{s}^{+}\times\boldsymbol{m}^{+})\cdot\boldsymbol{s}^{-}$ is always non-negative but $(\boldsymbol{s}^{+}\times\boldsymbol{m}^{+})\cdot\boldsymbol{m}^{-}$ is always zero. This is also true for $(\boldsymbol{s}^{-}\times\boldsymbol{m}^{-})\cdot\boldsymbol{m}^{+}$. Hence these slip system laminates are non-degenerate. For $(0\bar{1}11)[\boldsymbol{c}+\boldsymbol{a}_2]$ slip in one domain (+) and $(10\bar{1}1)[\boldsymbol{c}+\boldsymbol{a}_3]$ slip in the other (−) and taking $\boldsymbol{R}^{+}=\boldsymbol{R}^{-}=\boldsymbol{I}$, $(\boldsymbol{s}^{+}\times\boldsymbol{m}^{+})$ is a non-rational vector, [−0.0694, −0.7115, 0.5286] and so $(\boldsymbol{s}^{+}\times\boldsymbol{m}^{+})\cdot\boldsymbol{s}^{-}$ is non-negative; so also are $(\boldsymbol{s}^{+}\times\boldsymbol{m}^{+})\cdot\boldsymbol{m}^{-}$, $(\boldsymbol{s}^{-}\times\boldsymbol{m}^{-})\cdot\boldsymbol{s}^{+}$ and $(\boldsymbol{s}^{-}\times\boldsymbol{m}^{-})\cdot\boldsymbol{m}^{+}$. Hence these kinds of slip system laminates are always non-degenerate.

The interfaces between degenerate domains can be subdivided into three:

4.2.2. Type 1 degenerate interfaces

Interfaces between coplanar slip systems with coincident normals, $\boldsymbol{m}^{+}=\boldsymbol{m}^{-}$, and different slip directions, $\boldsymbol{s}^{+}\neq\boldsymbol{s}^{-}$. The interface in this case must be a rational crystallographic plane but the gross slip direction is non-rational. Degenerate domains with these characteristics have $\boldsymbol{R}^{+}=\boldsymbol{R}^{-}\equiv\boldsymbol{R}$, $\boldsymbol{N}=\boldsymbol{m}^{+}=\boldsymbol{m}^{-}\equiv\boldsymbol{m}$, $\boldsymbol{s}^{+}\neq\boldsymbol{s}^{-}$, and $\boldsymbol{a}=\gamma^{+}\boldsymbol{s}^{+}-\gamma^{-}\boldsymbol{s}^{-}$ where $\boldsymbol{a}$ is the vector in the compatibility equation (10). The slip activities, $\gamma^{\pm}$, are not constrained by the geometry alone. An example is an (0001) interface with $\boldsymbol{s}^{+}=[\mathbf{a}_1]$ and $\boldsymbol{s}^{-}=[\mathbf{a}_2]$ as shown in Fig. 16(a). Rational basal deformation lamellae presumably belong to this category. However effective $\langle\mathbf{c}\pm\mathbf{a}\rangle$ slip could arise from a degenerate process also. The situation would correspond to a common slip plane such as $m_1(01\bar{1}0)$ with slip parallel to $[+\mathbf{a}_1]$ in one domain and slip parallel to [+**c**] in the adjacent domain. If the resolved shear stress on both slip directions was similar then a package of laminations with a prism slip plane and with apparent $[\mathbf{c}+\mathbf{a}_1]$ slip would arise.

4.2.3. Type 2 degenerate interfaces

Interfaces between systems with coincident slip systems, $\boldsymbol{s}^{+}=\boldsymbol{s}^{-}$, and different normals, $\boldsymbol{m}^{+}\neq\boldsymbol{m}^{-}$. The interface in this case which is parallel to $\boldsymbol{s}^{+}$ can be a non-rational plane crystallographically but the gross slip direction is rational and equal to $\boldsymbol{s}^{+}$. We propose that this is the origin of many "irrational deformation lamellae" observed in naturally and experimentally deformed quartz although perhaps some arise as non-degenerate boundaries. Non-rational "slip" features are also observed in metals arising from such processes (Dmitrieva et al., 2009). An example is shown in Fig. 12(b) where the slip system in one domain is basal $[\mathbf{a}_1]$ and is prism $[\mathbf{a}_1]$ in the other. These kinds of domains are characterised by $\boldsymbol{R}^{+}=\boldsymbol{R}^{-}\equiv\boldsymbol{R}$, $\boldsymbol{s}^{+}=\boldsymbol{s}^{-}\equiv\boldsymbol{s}$, $\boldsymbol{a}=\|\gamma^{+}\boldsymbol{m}^{+}-\gamma^{-}\boldsymbol{m}^{-}\|\boldsymbol{s}$, and

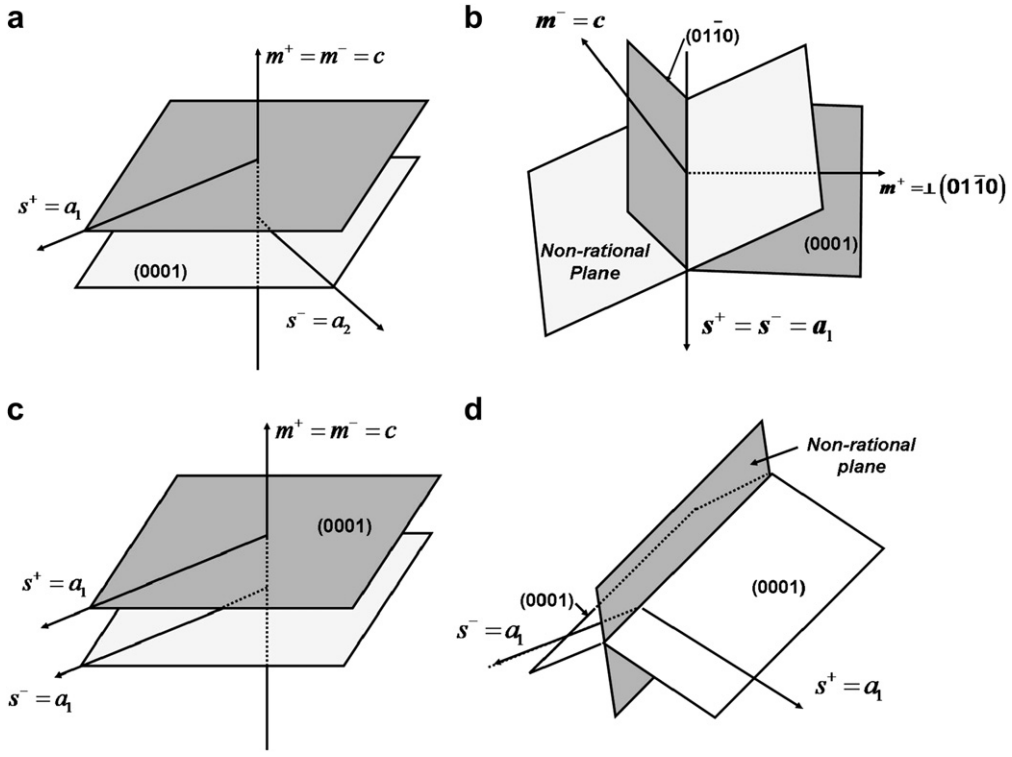

Fig. 12. Degenerate domain systems are slip packets with a common slip element in each domain. (a) Two parallel basal slip planes with different **a**-axes for slip. The boundary is rational. (b) Two different prism slip planes with a common **a**-axis for slip. The boundary is non-rational. (c) Two parallel basal slip planes with an identical **a**-axis for slip but different shears in each domain. The boundary is rational. (d) Basal slip in each domain and an identical **a**-axis for slip but different rotations either side of a non-rational boundary. See text for discussion.

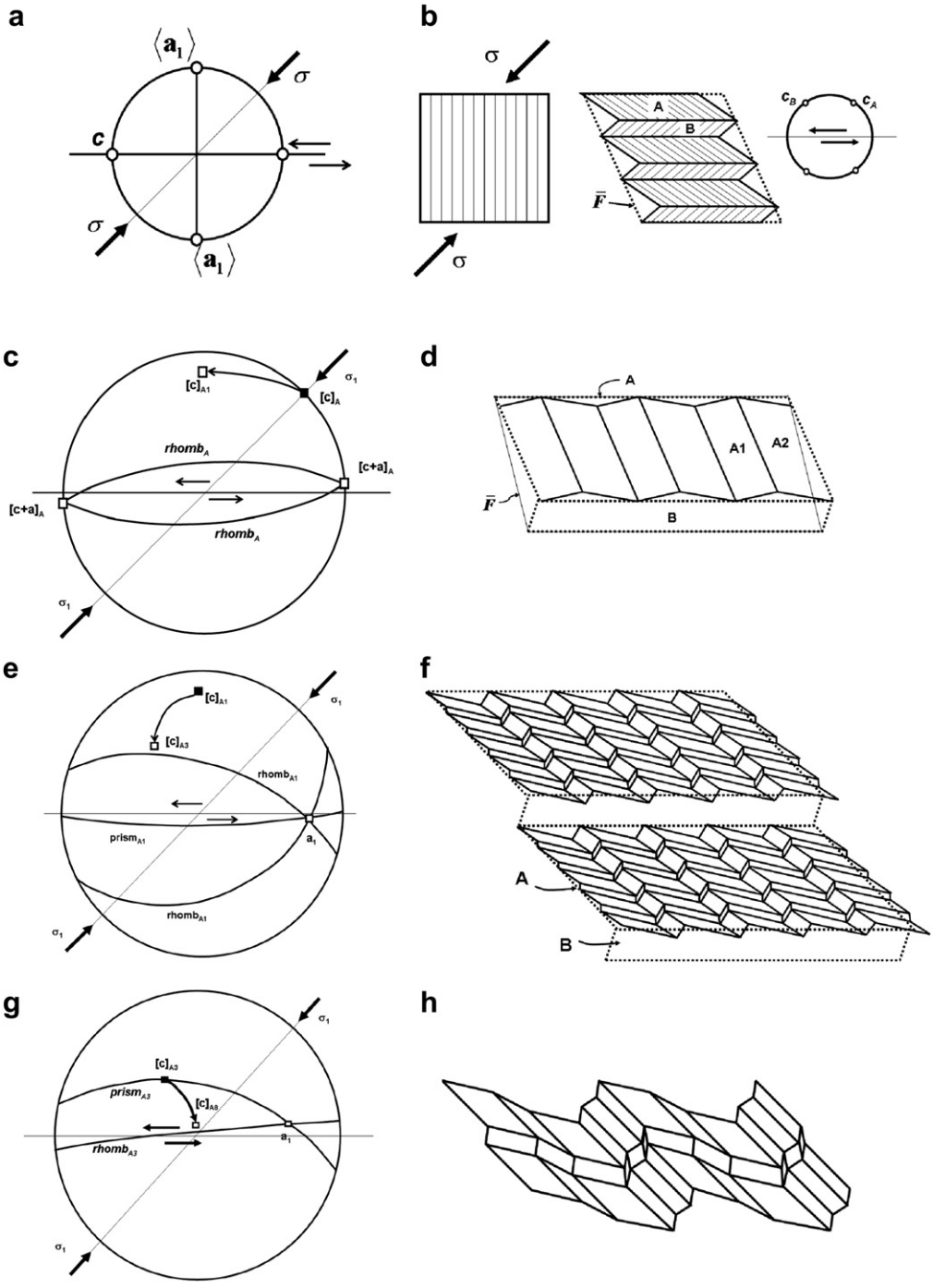

Fig. 13. A model for rotation recrystallisation. Development of domainal structures in Domain A. Projections are upper hemisphere equal area projections following Linker et al. (1984). (a) Initial orientation of lattice with basal slip parallel to $\langle \mathbf{a}_1 \rangle$ oriented at 45° to the compression axis $\boldsymbol{\sigma}$. The imposed slip deformation is sinistral with the slip direction horizontal in the projection. (b) The imposed average deformation is represented by $\overline{\boldsymbol{F}}$ and geometrical softening results in kinking to form the two domains A and B with orientations of the **c**-axis, $\mathbf{c}_A$ and $\mathbf{c}_B$ respectively. The volume proportion of A domains is larger than that of B domains to approximately accommodate $\overline{\boldsymbol{F}}$. (c) The pole $[\boldsymbol{c}]_A$ places $[\boldsymbol{c} + \mathbf{a}_1]$ close to the imposed slip direction and two rhomb planes close to the imposed slip plane. The resolved shear stress on these rhomb $\langle \mathbf{c} + \mathbf{a} \rangle$ systems is high; $[\boldsymbol{c}]_A$ rotates to $[\boldsymbol{c}]_{A1}$ (d) Domainal structure resulting from (c). The two domains A1 and A2 each have a different rhomb $\langle \mathbf{c} + \mathbf{a} \rangle$ slip system, as shown in (c), but can approximately accommodate the deformation represented by the parallelogram A. The evolution of domain B is treated in Fig. 14. (e) In the next stage of refinement $[\boldsymbol{c}]_{A1}$ places an **a**-axis close to the imposed slip direction and high resolved shear stress on a prism $\langle \mathbf{a} \rangle$ and two rhomb $\langle \mathbf{a} \rangle$ systems; $[\mathbf{c}]_{A1}$ is rotated to $[\mathbf{c}]_{A3}$. For details of the relations of the A domains see Fig. 15. (f) Domainal structure resulting from (e). The domains A1 and A2 in (d) are subdivided into domains with the different rhomb $\langle a \rangle$ systems shown in (e) operating. (g) In the next stage of refinement $[\mathbf{c}]_{A3}$ is rotated to $[\mathbf{c}]_{A8}$ placing the **c**-axis approximately normal to the imposed slip direction in the slip plane. (h) The resulting domainal structure. Details are given in Fig. 15. See text for discussion.

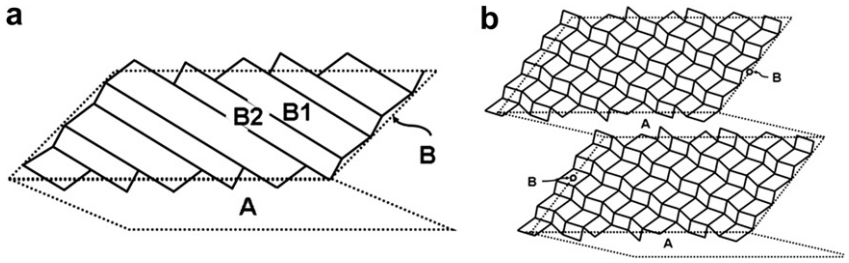

Fig. 14. The development of domainal structures in Domain B. Domain B in Fig. 13 is first divided into domains B1 and B2 to approximate the deformation in domain B. (b) Further refinement results in the microstructure shown. Details are given in Fig. 15. See text for discussion.

$$\boldsymbol{N} = \frac{\gamma^{+}\boldsymbol{m}^{+} - \gamma^{-}\boldsymbol{m}^{-}}{\|\gamma^{+}\boldsymbol{m}^{+} - \gamma^{-}\boldsymbol{m}^{-}\|} \tag{14}$$

where $\|\boldsymbol{A}\|$ stands for the norm of the vector $\boldsymbol{A}$ given by $\|\boldsymbol{A}\| = \sqrt{\sum_{i=1}^{n} A_i^2}$. Thus the compatible interface between a domain (+) with (0001)[$\mathbf{a}_1$] slip system and another (−) with $(01\bar{1}0)[\mathbf{a}_1]$ slip has an orientation given by

$$N_1 = 0,\ N_2 = \gamma^{-}/\sqrt{\gamma^{+2} + \gamma^{-2}},\ N_3 = \gamma^{+}/\sqrt{\gamma^{+2} + \gamma^{-2}} \tag{15}$$

so that if $\gamma^{+} = 10\gamma^{-}$ $\boldsymbol{N}$ is the vector [0, 0.0995, 0.995] which means the boundary is close to the basal plane (inclined at approximately 6°) and is clearly non-rational; this boundary is similar in orientation to the "sub-basal" lamellae described by McLaren et al. (1970). If we change the slip activity to be $\gamma^{+} = \gamma^{-}$ then $\boldsymbol{N}$ is the vector $[0, 1/\sqrt{2}, 1/\sqrt{2}]$. Again the boundary is non-rational but corresponds approximately to $\pi(01\bar{2}2)$ and is similar in orientation to some of the planar structures reported by Twiss (1976). The geometry of some common degenerate subgrain boundaries of this type to be expected in quartz is given in Table 4. This shows that boundaries involving these slip systems will always be parallel to [$\mathbf{a}_1$] but will be non-rational. For instance boundaries involving $(01\bar{1}0)[\mathbf{a}_1]$ and $(0\bar{1}11)[\mathbf{a}_1]$ slip are approximately 5° off $m_1(01\bar{1}0)$ for $\gamma^{+}_{(01\bar{1}0)} = 10\gamma^{-}_{(0\bar{1}11)}$ and approximately 25° off $m_1(01\bar{1}0)$ for $\gamma^{+}_{(01\bar{1}0)} = \gamma^{-}_{(0\bar{1}11)}$. These kinds of boundaries are expected to be common in quartz microfabrics developed by rotation recrystallisation at high shear strains as discussed below.

4.2.4. Type 3 degenerate interfaces

Interfaces between domains with identical slip systems, $\boldsymbol{s}^{+} = \boldsymbol{s}^{-}$ and $\boldsymbol{m}^{+} = \boldsymbol{m}^{-}$ but different shear strains in each domain, $\gamma^{+} \neq \gamma^{-}$. Both the interface and the gross slip direction are rational. An example where both the interface and the gross slip direction are rational is shown in Fig. 12(c) where the slip system in both domains is basal [$\mathbf{a}_1$]. If the domains are arranged as shown in

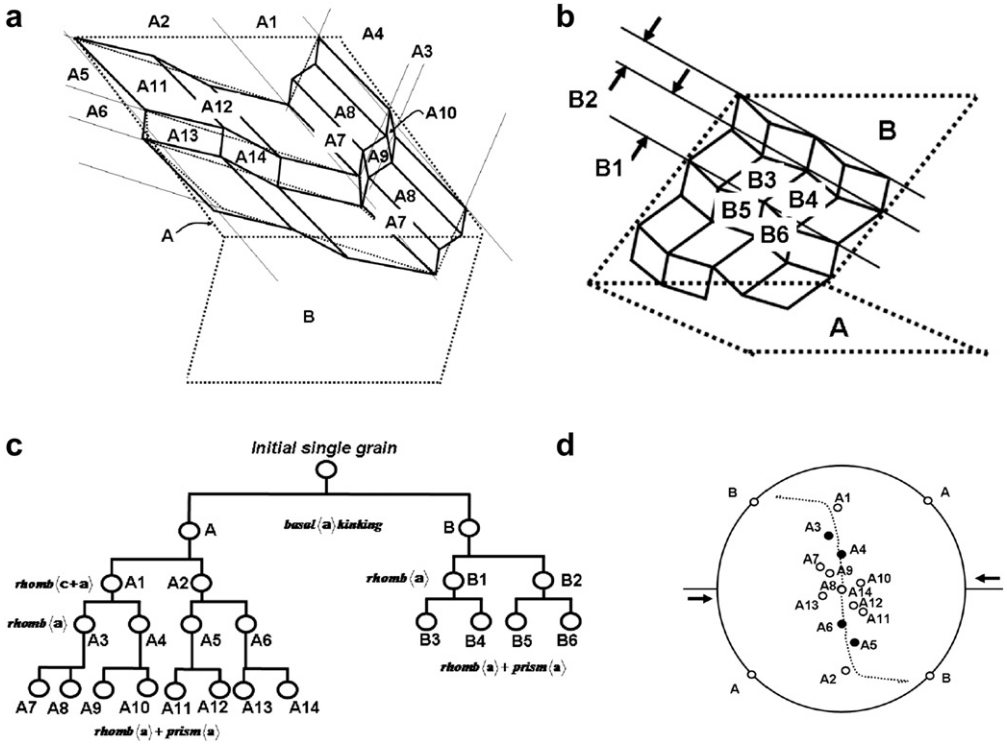

Fig. 15. A model for rotation recrystallisation. (a) Summary of domains developed in Domain A. (b) Summary of domains developed in Domain B. (c) The resultant tree structure. (d) Skeleton of resulting CPO with A-domains labelled.

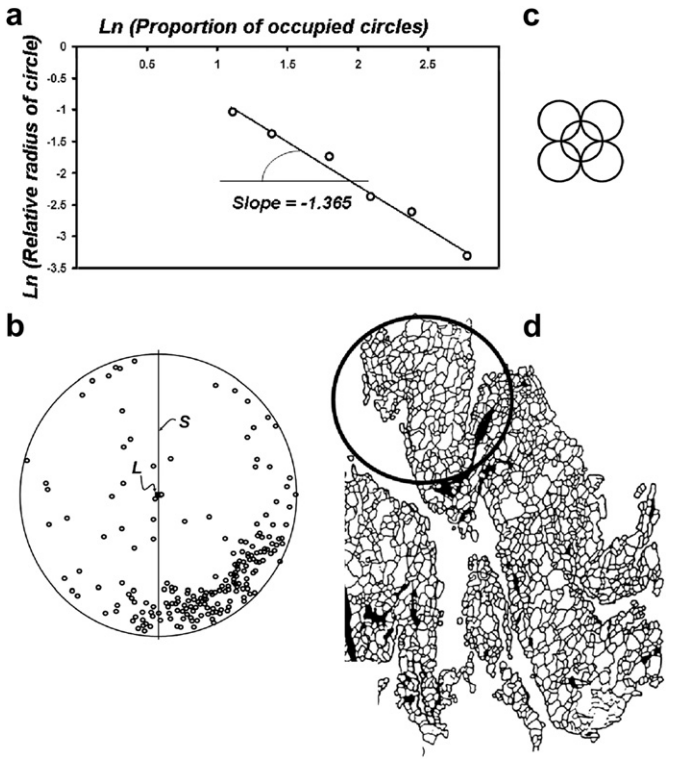

Fig. 16. Fractal nature of CPO. (a) Fractal dimension for plot in (b). Lower hemisphere equal area plot of 200 quartz **c**-axes. (c). "Unit cell" of circular counting array used to count c-axes in the equal area projection and to determine fractal dimension of (b). (d) Microstructure of sample showing area represented by (b). Data from Hobbs (1966).

Fig. 12(d) then a kink system is developed and the domain boundary is non-rational. Again the slip system in both domains is basal $[\mathbf{a}_1]$.

4.3. Simple laminates

Simple lamination of any of the single slip domains above enables a single crystal to achieve a larger range of deformation gradients than is possible with single slip in a homogeneous domain. For instance if $\boldsymbol{m}^+ = \boldsymbol{m}^-$ and $\boldsymbol{s}^+ \neq \boldsymbol{s}^-$, the interface must be the rational crystallographic plane whose normal is $\boldsymbol{m}$, but the gross slip direction can be non-rational. Thus the mean shear, $\overline{\gamma}$, and the effective slip vector, $\overline{\boldsymbol{s}}$, are given by:

$$\overline{\gamma} = \left\| \alpha^+\gamma^+\boldsymbol{s}^+ + \alpha^-\gamma^-\boldsymbol{s}^- \right\| \text{ and } \overline{\boldsymbol{s}} = \frac{\alpha^+\gamma^+\boldsymbol{s}^+ + \alpha^-\gamma^-\boldsymbol{s}^-}{\|\alpha^+\gamma^+\boldsymbol{s}^+ + \alpha^-\gamma^-\boldsymbol{s}^-\|} \tag{16}$$

4.3.1. The bulk deformation is given by

$$\overline{\boldsymbol{F}} = \boldsymbol{R}(\boldsymbol{I} + \overline{\gamma}\overline{\boldsymbol{s}} \otimes \boldsymbol{m}) \tag{17}$$

Table 4
Some common degenerate subgrain boundaries for quartz.

Slip system in (+) domain	Slip system in (−) domain	$\boldsymbol{N}$
$(0001)[\mathbf{a}_1]$	$(01\bar{1}0)[\mathbf{a}_1]$	$[0, \gamma^-/\sqrt{\gamma^{+2}+\gamma^{-2}}, \gamma^+/\sqrt{\gamma^{+2}+\gamma^{-2}}]$
$(0001)[\mathbf{a}_1]$	$(01\bar{1}1)[\mathbf{a}_1]$	$[0, 0.7857\gamma^-/M, (\gamma^+ \text{-} 0.6187\gamma^-)/M$
		$M = \sqrt{(\gamma^{+2} - 1.2374\gamma^+\gamma^- + \gamma^{-2})}$
$(01\bar{1}0)[\mathbf{a}_1]$	$(0\bar{1}11)[\mathbf{a}_1]$	$[0, (\gamma^+ \text{+} 0.7857\gamma^-)/M, -0.6187\gamma^-/M$
		$M = \sqrt{(\gamma^{+2} + 1.574\gamma^+\gamma^- + \gamma^{-2})}$

Clearly by varying the slip activities $\gamma^{\pm}$ and their volume fractions $\alpha^{\pm}$ any effective slip direction may be achieved.

4.3.2. Similarly, for laminates in which $\boldsymbol{m}^+ \neq \boldsymbol{m}^-$ and $\boldsymbol{s}^+ = \boldsymbol{s}^-$, the mean shear and the normal to the laminated system are

$$\overline{\gamma} = \left\| \alpha^+\gamma^+\boldsymbol{m}^+ + \alpha^-\gamma^-\boldsymbol{m}^- \right\| \text{ and } \overline{\boldsymbol{m}} = \frac{\alpha^+\gamma^+\boldsymbol{m}^+ + \alpha^-\gamma^-\boldsymbol{m}^-}{\|\alpha^+\gamma^+\boldsymbol{m}^+ + \alpha^-\gamma^-\boldsymbol{m}^-\|} \tag{18}$$

The interface must be a non-rational crystallographic plane and the slip direction is rational. By varying the slip activities, $\gamma^{\pm}$, and their volume fractions any non-rational laminate could result. The bulk deformation is given by

$$\overline{\boldsymbol{F}} = \boldsymbol{R}(\boldsymbol{I} + \overline{\gamma}\boldsymbol{s} \otimes \overline{\boldsymbol{m}}) \tag{19}$$

4.4. A model for rotation recrystallisation

Rotation recrystallisation evidently does not involve the nucleation of new grains that grow at the expense of stored or surface energies but instead involves the progressive rotation of subgrains with respect to the deformed initial grain so that large lattice rotations can be achieved with no subgrain growth necessary. Of course in many cases growth has occurred; we do not specifically consider these growth effects here but discuss the implications of boundary migration below and in Section 5.2. As far as we are aware the first experimental demonstration of rotation recrystallisation was by Hobbs (1968, pp. 386–391) who described the process as: "one in which adjacent subgrains increase their relative orientations during deformation until an array of highly misoriented grains is developed". Relative rotations with respect to the deformed initial grain of 90° were recorded although local misorientations are never larger than ~20°. The aim of this discussion is to produce a mechanism that accounts for such observations.

There seems to be no firmly established theory for the development of rotation recrystallisation although the process apparently involves crystal slip mechanisms because the resultant grains commonly have a single slip system aligned with both the inferred or observed shearing plane and shearing direction in a non-coaxial deformation history (Bouchez, 1978; Bouchez et al., 1983; Schmid and Casey, 1986; Dell'Angelo and Tullis, 1989; Schmid, 1994; Pauli et al., 1996; Heilbronner and Tullis, 2006). The CPO that develops at high strains by rotation recrystallisation is stronger and better defined than the CPO in the un-recrystallised grains in the same material (Heilbronner and Tullis, 2006). There are many papers that shed light on how the process may work (Hobbs, 1968; White, 1973, 1977; Poirier and Nicolas, 1975; Guillope and Poirier, 1979; Schmid et al., 1980; Tungatt and Humphreys, 1981; Garcia Celma, 1982; van Daalen et al., 1999; Jiang et al., 2000; Bestmann and Prior, 2003; Halfpenny et al., 2006; Stipp and Kunze, 2008).

We outline below the beginnings of a theory of rotation recrystallisation in quartz based on the proposals and observations made in the literature above and emphasise the proposal by Ortiz and Repetto (1999) that the development of sequential laminates is to be expected in systems undergoing single slip because such a development minimises the Helmholtz energy in the system. Such a proposal has been experimentally confirmed by Dmitrieva et al. (2009) with the analysis of experimentally developed non-rational lamellae in copper. In what follows we use the term *recrystallisation* to mean solely rotation recrystallisation with no grain-growth that is driven by Helmholtz energy or surface energy effects. Grain (and subgrain) boundaries can migrate during the

recrystallisation process described below but the reason is solely to maintain compatibility of grain deformation with the imposed deformation and with the deformation in adjacent domains.

We briefly summarise the proposals put forward by Ortiz and Repetto (1999) and some subsequent work by Miehe et al. (2004) before presenting a model for rotation recrystallisation. Firstly, geometrical softening and latent hardening lead to non-convex Helmholtz energy functions so that it is energetically favourable to develop a domainal structure comprising regions of single slip rather than deform homogeneously with several slip systems operating simultaneously throughout. Secondly, in order to achieve compatibility with the imposed deformation gradient, nine (eight if the deformation is prescribed as isochoric) independent deformations must be present in order to match the nine components of the imposed deformation gradient. One can see that these two propositions already have the potential to produce interesting microfabrics because the development of at least eight domains each characterised by single slip systems and each associated with its own lattice rotation already has the hallmarks of rotation recrystallisation. Thirdly, the domain boundaries are of two types labelled non-degenerate and degenerate. With continued deformation, non-degenerate boundaries require rotation within the adjacent domains in order to maintain compatibility across the boundary. Degenerate boundaries require no rotation. Domain boundaries can be crystallographically rational or non-rational; their geometry is not arbitrary but is clearly defined by the deformation in adjacent domains. Fourthly, the model proposes that strict compatibility with the imposed deformation gradient in general requires a self similar refinement of the microstructure somewhere in the deformation geometry although this may become unimportant at high strains (Miehe et al., 2004). Fifthly, by varying the amount of slip activity in each domain and the volume fractions of the domains, a wider range of deformations can be matched than by single slip either side of the boundary. These principles were developed by Ortiz and Repetto (1999) for deformation histories where the microstructure is frozen early in the deformation history and remains static throughout the history and were applied to the development of subgrains by Ortiz et al. (2000). An advance was made by Miehe et al. (2004) who extended the theory to include progressive evolution of a two-dimensional bi-domainal microstructure. Further advances have been made by Hansen et al. (2010). They show that as the deformation proceeds the volume fraction of the two domains can change so that for some deformation histories the geometry evolves so that only one domain comprised of single slip survives and is capable of matching the imposed deformation gradient. This means that the domain boundaries migrate during the deformation history and the size and shape of domains also evolves. The work by Miehe et al. (2004) and Hansen et al. (2010) seems to represent the state of the art in this area but further development is necessary to be able to simulate the evolution of more complicated microfabrics. It is important to stress that the size and shape of the subgrains evolves with increasing deformation.

The literature reveals many direct correlations between the above five propositions and observations made on quartz CPO development. We take two examples, namely, Schmid and Casey (1986) and Heilbronner and Tullis (2006). Schmid and Casey (1986) emphasise that inhomogeneous deformation in which domains of distinct crystallographic orientation develop is an essential part of the CPO development process in naturally deformed quartz rich rocks. They present compelling evidence for single slip dominating in individual domains within the microstructure. In particular slip parallel to ⟨**a**⟩ and the alignment of one of the **a**-axes with a shearing direction is presented as the dominant mechanism in CPO development. Recrystallisation by a subgrain rotation mechanism is presented as a concurrent contributing mechanism with crystal plastic mechanisms playing a dominant role in controlling the orientation of the recrystallised grains.

Heilbronner and Tullis (2006) determined the evolution of the **c**-axis fabrics for a quartzite experimentally deformed in a plane strain deformation history that was dominantly simple shearing with minor shortening normal to the shearing plane. The observations supplement those of Schmid and Casey (1986). A distinct domainal structure develops that has a length scale different from the initial grain size. As the shear strain increases the individual domains are dominated by single slip systems that can, on average, accommodate the imposed incremental deformation. Also with increasing shear strain there is a progression from a situation where grains with basal ⟨**a**⟩ and rhomb ⟨**a**⟩ systems are present to microfabrics dominated by rhomb ⟨**a**⟩ slip through to microfabrics dominated by grains where prism ⟨**a**⟩ slip can achieve the imposed deformation but rhomb ⟨**a**⟩ slip is still present (their Fig. 10). The patterns at high strains arise progressively by the elimination of basal ⟨**a**⟩ domains so that there is a transition sequence

$$\text{basal}\langle\mathbf{a}\rangle \rightarrow \text{basal}\langle\mathbf{a}\rangle + \text{rhomb}\langle\mathbf{a}\rangle \rightarrow \text{rhomb}\langle\mathbf{a}\rangle \rightarrow \text{prism}\langle\mathbf{a}\rangle + \text{rhomb}\langle\mathbf{a}\rangle$$

The recrystallised grains show the strongest preferred orientations whereas the “old grain” remnants show a related but weaker CPO where the prism ⟨**a**⟩ orientations are not as well developed. The percentage recrystallised and the rotation of the fabric skeleton relative to the shearing direction increase with increasing shear strain.

Below we present a model based on these observations that proposes a domainal microstructure that is compatible with the principles discussed by Ortiz and Repetto (1999). The basic premise is that geometrical softening and/or latent hardening induce single slip in parts of a grain so that inhomogeneous deformation results. This represents a configuration that minimises the Helmholtz energy of the system. The pattern of inhomogeneous deformation is arranged so as to achieve compatibility with the imposed deformation gradient. This is the inverse way of considering the situation to Schmid (1994) who proposed that recrystallisation weakens grain boundary constraints to allow grains to undergo single slip. The Ortiz-Repetto model proposes that single slip is preferred for energetic reasons and that rotation recrystallisation enables compatibility with the imposed deformation to be achieved. Notice that both the approach used here and the Taylor-Bishop-Hill approach appeal to energy extremum principles. The Taylor formulation of the problem is: *Given five independent slip systems that operate simultaneously, what combination of shears on these systems will minimise the work done assuming that the incremental strain in every grain is the same as the imposed increment of strain?* The problem reformulated for rotation recrystallisation is: *Given an imposed deformation gradient, what spatial arrangements of deformation gradients arising from single slip will guarantee deformation compatibility between grains and sub-grains together with compatibility with the imposed deformation and at the same time minimise the Helmholtz energy of the system?*

At the present time it is not possible to provide an answer to the rotation recrystallisation question posed above in the sense that a computer program could be executed to simulate both microstructural and CPO development although the papers by Miehe et al. (2004) and Hansen et al. (2010) begin to explore such models. This is because it is not possible at present to uniquely predict the precise microstructure that will minimise the Helmholtz energy and the ways in which this microstructure will evolve with time; the microstructures modelled in martensitic (Ball and

James, 1987) and metal plasticity problems (Ortiz et al., 2000) do not evolve during a simulation but are postulated by analogy with observed microstructures. As indicated above, first steps in this direction have been taken by Ortiz et al. (2000), Miehe et al. (2002) and Hansen et al. (2010). However it is possible to work through examples that illustrate the principles involved.

As one example we take a grain with an initial orientation shown in Fig. 13(a) in a sinistral simple shearing deformation history. The gross deformation is a bulk plane straining with the bulk shear direction constantly oriented in time as shown in Fig. 13 (a). We choose this orientation as an example because this orientation, and others nearby, requires the maximum number of laminates or domains to form in order to reach a steady state configuration that simultaneously accommodates the imposed deformation and minimises the Helmholtz energy of the system. Both [**c**] and [$\mathbf{a}_1$] are at 45° to σ_1 so that basal [$\mathbf{a}_1$] slip is favoured (resolved shear stress, RSS = 0.5). Geometrical softening leads to kinking in order to minimise the Helmholtz energy and produces domains A and B as shown in Fig. 13(b). The volume fractions of A and B domains are different in order to accommodate the average imposed deformation, $\overline{\boldsymbol{F}}$. Domain A now has high resolved shear stress on all rhomb $\langle \mathbf{c} \pm \mathbf{a} \rangle$ systems (RSS = 0.45). In particular, $r_2(10\bar{1}1)$ and $r_3(\bar{1}101)$ have$\langle \mathbf{c} \pm \mathbf{a} \rangle$ slip directions in the plane of deformation (Fig. 13(c)) and between them can contribute to a non-degenerate laminate with a gross slip direction almost parallel to the bulk shear direction. In order to minimise energy we propose that geometrical softening and/or latent hardening produces a second domainal structure (A1 and A2) as shown in Fig. 13(d) in which these two different rhomb $\langle \mathbf{c} \pm \mathbf{a} \rangle$ systems operate. Notice that other closely oriented grains will have rhomb systems with slightly different orientations so that between them they can produce an average deformation that approximates the imposed bulk deformation.

The development of A1 and A2 domains both associated with slip on a positive or negative rhomb in a $\langle \mathbf{c} \pm \mathbf{a} \rangle$ direction places basal [$\mathbf{a}_1$] and rhomb [$\mathbf{a}_1$] systems into orientations with high resolved shear stress and so that [$\mathbf{a}_1$] is approximately parallel to the shearing direction (Fig. 13(e)). The resolved shear stress is highest on the base (approximately 0.47) and marginally less on the rhombs (of the order of 0.45) so that new laminate structures (A3 + A4 and A5 + A6) can form employing these slip systems individually (see Fig. 15). The decision on what actually happens is governed by the critical resolved shear stress for these systems which in turn is a function of the temperature and strain-rate. We suppose that temperature conditions are such that only the rhombs operate. The A3 + A4 and A5 + A6 domains have symmetrically related slip systems (Figs. 13(f) and 15) so that laminates comprised of both domains are capable of approximating the bulk shearing deformation.

In all of the domains A3–A6 the resolved shear stress is now high on both rhomb [$\mathbf{a}_1$] and prism [$\mathbf{a}_1$] systems (Fig. 13(g)) and new laminates (A7–A14) form as shown in Fig. 13(h). Further slip on the prism [$\mathbf{a}_1$] system does not alter the orientation of **c**, since **c** is now the axis of rotation of the lattice, but operation of the rhomb [$\mathbf{a}_1$] system progressively rotates [**c**] towards the normal to the bulk slip direction in the plane of bulk shearing so that ultimately only the prism [$\mathbf{a}_1$] system operates and all other laminates decrease in volume. This represents a steady state orientation, at least for [**c**], and the bulk imposed deformation can now be accommodated by prism [$\mathbf{a}_1$] slip alone although some self similar refinement is needed to be fully compatible with the imposed bulk deformation. Such refinement may be expressed as a diffuseness in the CPO rather than a change in subgrain size.

For the B domain shown in Fig. 13(b) the route to a steady state orientation is somewhat shorter. This part of the grain is rapidly placed in an orientation for rhomb [$\mathbf{a}_1$] slip by basal [$\mathbf{a}_1$] kinking, in which only one kinked domain is capable of accommodating the imposed deformation by basal $\langle \mathbf{a} \rangle$ slip, and then follows the route already outlined for part A of the grain. The sequence of laminate development is shown in Fig. 14 and the final steady state prism [$\mathbf{a}_1$] orientation together with rhomb [$\mathbf{a}_1$] is developed.

The resulting units of the microstructure are shown in Fig. 15 (a) and (b). The tree structure which describes this domainal structure is shown in Fig. 15(c) and as a whole consists of 12 leaves and 11 internal nodes. This means that the refining of the microstructure results in 15 degrees of freedom which, for an isochoric deformation gradient is more than the 8 degrees of freedom necessary for gross compatibility. Grains of other initial orientations require fewer levels of refinement and although the number of degrees of freedom may exceed that necessary to produce compatibility with the imposed deformation the number that actually develop for a given initial orientation is that required both to accommodate the imposed deformation and to reach a steady state orientation. By definition, at steady state, no further refinement by laminate development occurs and the Helmholtz energy of the system has therefore reached a minimum. The resulting CPO skeleton for the A domains is shown in Fig. 15(d). This skeleton acts as an attractor for all initial orientations in the system and represents all those crystallographic orientations that together can accommodate the imposed deformation and minimise the Helmholtz energy of the system. Notice that as one moves down the tree the domains with prism $\langle \mathbf{a} \rangle$ and rhomb $\langle \mathbf{a} \rangle$ slip dominate as is observed in the experiments of Heilbronner and Tullis (2006). This progression down the tree corresponds to the development of an asymmetrical girdle with a concentration of **c**-axes normal to the bulk slip direction in the plane of shearing through the sequence:

$$\text{basal}\langle \mathbf{a} \rangle \rightarrow \text{basal}\langle \mathbf{a} \rangle + \text{rhomb}\langle \mathbf{a} \rangle \rightarrow \text{rhomb}\langle \mathbf{a} \rangle \rightarrow \text{prism}\langle \mathbf{a} \rangle + \text{rhomb}\langle \mathbf{a} \rangle$$

The boundaries of subgrains formed in this process are both degenerate and non-degenerate. Those boundaries that are parallel to a common slip direction are type 2 degenerate boundaries that are non-rational and require no rotation to maintain deformation compatibility across them. Their orientations are given by Equation (18). Those boundaries that are oblique to both slip planes and slip directions either side of the boundary are non-degenerate boundaries that require further rotation across them as deformation proceeds in order to maintain deformation compatibility. Their orientations can be calculated using Equation (11) along with the rank-1 compatibility relation (10).

4.5. Fractal CPO's

The development of sequential laminates involves a self similar subdivision of the microstructure as shown by the tree structures in Fig. 10(a) and 15(c). This produces a microstructure where broad compatibility with the imposed deformation gradient can be achieved by single slip in each laminate. In addition, a self similar refinement is required to fill in the gaps in this broad microstructure as shown in Fig. 9. This suggests that the microfabric may be fractal and that this could be reflected in the CPO. The self similar subdivisions and refinements reflected in the tree structures are reminiscent of the formation of Cantor dust in one dimension, Koch curves in two dimensions and a Sierpinski gasket in three dimensions (Mandelbrot, 1983). The microfabric in two dimensions has close affinities with the non-re-entrant dyadic Koch curve and so

we expect a fractal dimension, f, such that $1 < f \leq 1.5$. The plot in Fig. 16(a) shows that for the CPO in Fig. 16(b) the fabric is indeed fractal with a fractal dimension of 1.365. This calculation was performed using arrays of overlapping circles (Fig. 16(c)) on the equal area projection of **c**-axes where the total array of circles just covered the projection and the number of circles occupied by at least one **c**-axis pole was counted for a range of circle diameters. Similar results were obtained with non-overlapping squares. There clearly is a need to examine the process of calculating the fractal dimension of CPO's and perhaps it should be done on the sphere. There is a wide seismological and astronomical literature on this subject (Kagan, 2007; Murdzek, 2007; Koenig and Chainais, 2008).

5. Discussion

5.1. The development of fabric

In this paper we have explored the proposal made by Ortiz and Repetto (1999) that the development of microstructure in plastically deforming materials is a response to minimise the Helmholtz energy in the system and we have extended the concept to the development of the complete microfabric. The Helmholtz energy is envisaged as a non-convex function of the deformation gradient so that a homogeneous deformation is not capable of minimising the energy whereas an array of differently deformed domains does minimise the energy. The concept in turn is based on a large volume of work on non-linear elastic systems (Ball and James, 1987; Silhavy, 1997; Bhattacharya, 2003). The approach has also been applied independently to the formation of kink and chevron folds (Hunt et al., 2001) and to the development of damage (Lyakhovsky and Ben-Zion, 2008) and fracture (Del Piero and Truskinovsky, 2001).

The problem is essentially one of developing compatibility in the deformation from one domain to another and such that the average deformation of the complete array of domains is compatible with the imposed deformation. Nine levels of refinement of the microstructure are required to match the nine independent components of the imposed deformation gradient matrix so that some complexity in the spatial arrangement is an outcome of the model. The refinement process comprises a self similar partitioning of the average deformation. However any array of finite sized domains can never match an imposed deformation so that a self similar array of finer and finer domains develops in order to fill the gaps. This ensures that any long range stresses are minimised. These self similar refinement processes introduce a fractal character to the microstructure geometry. If the self-similar refinement is also thought of as a scatter in the CPO then a fractal character is expected of the CPO also.

Understanding the lower limit in size for these refinement processes has been recognised as a problem for over 30 years (Ericksen, 1975; Truskinovsky and Zanzotto, 1996; Bhattacharya, 2003). One way of arriving at a lower limit to the size of refinement is to introduce the surface energy of the boundaries of domains within the microstructure as an intrinsic part of the minimisation process (Bhattacharya, 2003). There is then a competition between *decreasing* the Helmholtz energy by increasing the number of domains and *increasing* the total energy of the system by increasing the number of surfaces. The lower length scale for the microstructure is then set when the increase in energy due to introducing new surfaces matches the decrease in energy due to formation of a new domain. It is clear that the magnitude of the Burgers vector also sets a lower limit and it is interesting that Twiss (1976) notes that domain boundaries may become fuzzy (the "laminae" of Twiss) and this may mark an environment where the dislocations have greater mobility and are not restricted to a single slip plane. The present paper has concentrated on microfabrics developed in deformed quartz aggregates but the arguments are just as applicable to a range of other microfabrics.

In particular we have not explored the concept of minimising the surface energy of microstructural boundaries in this paper but it is clearly a fundamental issue in controlling the shapes and sizes of microstructural elements. In particular the formation of foliations and mineral lineations by metamorphic differentiation takes on a new light. In particular the comprehensive work by Ortoleva (1989) and co-workers Ortoleva et al. (1982) proposes that metamorphic differentiation arises because of the non-linear interactions between the kinetics of competing mineral reactions. His approach is similar to other work in pattern formation arising from non-linear chemical kinetics (Epstein and Pojman, 1998) which is commonly expressed as some form of reaction-diffusion equation (Cross and Hohenberg, 1993). Ortoleva's contribution has been to recognise (based on an important paper by Ortoleva and Ross, 1974) that even the simplest of mineral reactions can become unstable if the system is heterogeneous in the sense that reaction sites are not homogeneously distributed but are controlled by the microstructure and/or localised deformation sites. This heterogeneity would seem to be characteristic of deforming metamorphic rocks.

The point that arises from this work is that the microstructural surfaces that develop in such systems and that mark the boundaries between compositional phases are surfaces that minimise the surface energy of the system (De Wit et al., 1997; Glimm and Hentschel, 2008). They are in fact minimal surfaces or surfaces that closely approach minimal surfaces in that they have zero mean curvature (Hobbs and Ord, in press). Thus we envisage that the development of microstructures such as foliations, cleavages, schistosities and mineral lineations by metamorphic differentiation processes is firstly a response to minimising the Helmholtz energy in the system by partitioning the deformation into domains and secondly an attempt to minimise the surface energy associated with the boundaries of the fabric domains.

5.2. CPO's

The main example we have explored in this paper is the development of crystallographic preferred orientation in quartz aggregates. The differences between the Taylor-Bishop-Hill approach and others that have been proposed are essentially the postulated mechanisms of ensuring or approximating compatibility with the imposed deformation and between adjacent deformation domains. The Taylor-Bishop-Hill approach ensures compatibility by insisting on the simultaneous operation of five independent slip systems so that any imposed deformation can be accommodated so long as the deformation is identical in each grain; this means that the deformation is homogeneous. This means also that deformation compatibility exists across grain boundaries of any orientation. In the model of Jessell and Lister (1990), grains are selectively removed by grain-boundary migration so that those that have experienced the maximum work vanish from the CPO. Since the strict Taylor-Bishop-Hill model lies in the background to this model, grain boundaries of any orientation are admissible. The Taylor-Bishop-Hill model is not physically realistic but the approach does explain many features of observed CPO's especially in metals when recrystallisation is absent (Bronkhorst et al., 1992). The approach due to Etchecopar (1977) and Etchecopar and Vasseur (1987) admits that incompatibilities will exist but attempts to minimise the effect. Nevertheless, significant gaps between grains and overlaps between grains remain in the Etchecopar approach implying the existence of long range stresses and discontinuities in the deformation. This approach also is not realistic physically but comes remarkably close to simulating some observed patterns of CPO. The self-consistent approach used by Wenk (1999) relaxes the constraint of homogeneous deformation and hence

allows deformation with fewer than five independent slip systems. In such a model the grain boundaries need to obey the compatibility condition (10). The approach proposed by Ortiz and Repetto (1999) is perhaps the most realistic so far developed. It proposes that deformation will be inhomogeneous in the sense that individual domains characterised by single slip develop to minimise the energy of the system. Deformation compatibility is enforced not only on average with the imposed deformation but locally between domains as well. The progressive refinement of microfabric together with the requirement for compatibility of deformation in general demands lattice rotations between differently deformed domains so that rotation recrystallisation emerges from this scheme as a natural consequence. We have presented a specific example of this process in this paper with respect to the development of an asymmetric girdle in a simple shearing deformation history. It is notable that the CPO can be developed by rotation recrystallisation using the Ortiz and Repetto approach without resort to five independent slip systems; slip systems employing [**c**] as a slip vector are not necessary in the example proposed.

A number of processes have been proposed for the development of recrystallised grains of quartz (Stipp et al., 2010). One (christened bulging recrystallisation; Drury et al., 1985; Hirth and Tullis, 1992; Stipp and Kunze, 2008) is proposed to arise from rotation of subgrains accompanied by grain-boundary migration (Stipp et al., 2010). A second (christened subgrain rotation recrystallisation; Hobbs, 1968; White, 1973; Guillope and Poirier, 1979) is dominated by subgrain rotation and a third (christened bulging recrystallisation; Hobbs, 1968; White, 1973; Guillope and Poirier, 1979) is dominated by grain boundary migration but presumably relies on subgrain rotation or some other mechanism (Halfpenny et al., 2006) in order to form the initial region for growth. In addition grain boundary sliding may be an important mechanism and twinning may be important in some instances (Stipp and Kunze, 2008). Some authors have postulated rigid body rotation or some form of granular flow that may or may not be accompanied by grain boundary sliding (van Daalen et al., 1999; Jiang et al., 2000; Bestmann and Prior, 2003; Halfpenny et al., 2006).

All of these mechanisms except those involving rigid body rotation and granular flow seem to be special cases of the model proposed here and we would interpret them as mechanisms to achieve compatibility of deformation across the recrystallised aggregate with progressive deformation of the aggregate. A model for the subgrain rotation mechanism (*sensu stricto*) is specifically addressed in this paper. However the model proposed here is to a large extent "static" in that the subgrain structure is modelled at successive instants during the deformation history. The development and implementation of models that can address the history of deformation and at the same time describe the sequential development of the microfabric have been long in development and are only just starting to appear (Miehe et al., 2002, 2004; Hansen et al., 2010) but the sequential evolution of the microfabric (as one would expect) involves changes in subgrain shapes and sizes and hence the migration of subgrain boundaries. In particular Miehe et al. (2004) show that although a diverse microstructure may form early in the deformation history, rotation of the lattice can result in a situation where compatibility of deformation with the imposed deformation is achieved ultimately by a single grain orientation. This means that grain boundary migration is a mechanism of both increasing the grain size and in producing compatibility of deformation. Similar results are presented by Hansen et al. (2010). This process of elimination of incompatible grains by grain boundary migration with the production ultimately of an array of grains compatible with the imposed deformation may represent the development of a stable, more or less homogeneous grain size even though the CPO remains fractal.

Grain boundary sliding can be a special mechanism for achieving compatibility of deformation across a grain or subgrain boundary. The compatibility condition (10) is a statement that discontinuities in the deformation between two subgrains are allowed only in the direction normal to the subgrain boundary. Discontinuities in the shear strain parallel to the boundary are allowed but need to be accommodated on the scale of the subgrain or smaller. Grain or subgrain boundary sliding is one way of achieving this aspect of deformation compatibility at a fine scale where the grain boundary becomes a shear zone. Thus boundary sliding is one way of achieving part of deformation compatibility across the boundary by subgrain refinement at a scale close to that of the boundary itself.

As indicated earlier the Taylor-Bishop-Hill approach has been remarkably successful in modelling the development of CPO's particularly in metals. Miehe et al. (2002) use the principle of minimising the Helmholtz energy to model CPO development in copper with the strict requirement of homogeneous strain imposed by the Taylor-Bishop-Hill approach relaxed to include periodic and stress boundary conditions. They model plane, axisymmetric and simple shearing deformation histories but with multiple slip allowed and compare the results with the experimental results of Bronkhorst et al. (1992). The results indicate that the strict Taylor-Bishop-Hill approach reproduces the experimental results closely but the CPO is much too sharp. The periodic and stress boundary conditions smear out the CPO. This study suggests that the strict Taylor-Bishop-Hill approach involving strict homogeneity in the imposed deformation is an upper bound to the diffuseness in the resulting CPO. We do not expect CPO's predicted by this approach to be fractal. As the boundary conditions are relaxed (as in the Miehe et al., 2002 study or as in the self-consistent methods used by Wenk, 1999) the CPO becomes more diffuse. In order to make fundamental changes to the CPO predicted by the Taylor-Bishop-Hill approach a fundamentally new deformation mechanism needs to be introduced and in this paper this has been proposed as geometrical softening (hardening) or perhaps latent hardening. This immediately enforces non-convexity in the Helmholtz energy so that microstructures have to develop in order to minimise the Helmholtz energy. The extra requirement of compatibility both locally and globally results in refinement of the microstructure which we interpret as rotation recrystallisation. Grain and subgrain migration (changes in the sizes and shapes of subgrains) are important ingredients of the evolution of the microfabric and conceivably grain-boundary sliding is also.

Other mechanisms of deformation include dislocation climb. Groves and Kelly (1969) show that this process can enable a general deformation without five independent slip systems and is responsible for a deformation gradient for climb of a set of identical edge dislocations, $\boldsymbol{F}^{climb}$, given by

$$\boldsymbol{F}^{climb} = I + \gamma^{climb}(\boldsymbol{s}\otimes\boldsymbol{s}) \tag{20}$$

where γ^{climb} is the dilation introduced through downward extension of the extra half plane of a dislocation with $\boldsymbol{s}$ as a unit vector parallel to the Burgers vector. This deformation by definition is not isochoric but an isochoric deformation can be produced by two or more different sets of dislocations undergoing simultaneous climb or by a single set climbing with access to a grain boundary diffusion flux. Thus the deformation gradient for combined slip and climb is

$$\boldsymbol{F}^{total} = \boldsymbol{F}^{climb}\boldsymbol{F}^{plastic} \tag{21}$$

where $\boldsymbol{F}^{plastic}$ is meant to be given by (11). This process simply reduces the number of required slip systems to achieve a given deformation and would be expected to smear out the result of a strict Taylor-Bishop-Hill analysis. The orientation of grain

boundaries for processes involving climb is not arbitrary and for compatibility must obey (10) where $\boldsymbol{F}$ is now identified with $\boldsymbol{F}^{total}$.

Thus processes such as climb, grain-boundary migration and some forms of grain-boundary sliding are expected to smear out the CPO predicted by a strict Taylor-Bishop-Hill approach and all lead to deformations where (10) needs to be obeyed for deformation compatibility.

The CPO development mechanism that derives from the work of Ortiz and Repetto (1999) implies that the CPO itself may be a fractal and we have shown one example of this (Fig. 16). The interesting aspect to explore is whether the fractal dimension of CPO's is useful in defining the physical conditions of deformation. It is clear that the degree of preferred orientation varies with amount of strain (Heilbronner and Tullis, 2006) and that temperature also influences the pattern of CPO (Law et al., 2004) in that the opening angle of crossed girdle fabrics varies with temperature. It is not yet clear that these differences in CPO are reflected in the fractal dimension of the CPO but visual inspection of the patterns suggests this is so. Clearly more work is needed. The argument we have presented supposes that for the most part the critical resolved shear stresses are the same on all activated slip systems. Changes in the relative critical resolved shear stresses with temperature, strain-rate and other parameters will govern the details of which domains develop and their relative proportions so that different CPO's will develop and presumably different fractal dimensions. As with the Taylor-Bishop-Hill approach, the Ortiz-Repetto approach prescribes that the CPO development is controlled by the kinematics of the deformation rather than by the strain that accumulates during the deformation history. This is what Sander (1911) proposed.

6. Concluding statement

This paper proposes that the microfabrics observed in deformed metamorphic rocks develop to minimise the total Helmholtz energy of the reacting-deforming system. Microfabrics do not develop unless the Helmholtz energy function is non-convex and such a form for the Helmholtz energy function is suggested by any stress–strain curve that shows softening. The development of microfabrics then follows by exactly the same chemical thermodynamic arguments that pertain to the development of two chemical phases in a two phase system (the Maxwell construction, Kondepudi and Prigogine, 1998, p. 193) and to the development of microstructures in finite non-linear elasticity (Ball and James, 1987; Truskinovsky and Zanzotto, 1996). The difference between this previous work and the present approach derives from the paper by Ortiz and Repetto (1999) who pointed out that the same principles can be applied to the development of microstructures during the plastic deformation of metals. Two additional aspects to microfabric development arise over and above minimisation of the Helmholtz energy. One involves the self similar refinement of a given coarse microstructure in order to achieve compatibility with the imposed deformation gradient. This process leads to fractal microstructures and, we propose, is the mechanism involved in the development of rotation recrystallisation. The process also implies that crystallographic preferred orientations should be fractal and an example of this is presented. The total microfabric of a deformed metamorphic rock is not to be viewed as a piecemeal assemblage of individual grains and grain segregations that define lineations and foliations unrelated to crystallographic preferred orientations and subgrain microstructures, but as a coherent, integrated structure that forms in order to minimise the Helmholtz energy of the system. As such the formation of each aspect of the microfabric is coupled to all other aspects. An important bi-product of such an argument is that the microfabrics we see in deformed metamorphic rocks form in response to the kinematics of deformation and not the geometry of the deformation as represented by the strain tensor as is a current dogma.

The present paper is an introduction to the interpretation of microfabrics as minimisers of Helmholtz energy. It is hoped that this work will stimulate detailed microstructural studies of rotation recrystallisation in which precise measurements of subgrain/grain boundary orientations together with precise measurements of the total crystallographic orientations either side of the boundaries to test whether the compatibility condition $\boldsymbol{F}^{+} - \boldsymbol{F}^{-} = \boldsymbol{a} \otimes \boldsymbol{N}$ is satisfied in naturally and experimentally deformed minerals. Such measurements need to be linked to the presumed kinematics of deformation to ascertain if the microfabric is kinematically consistent or if modifications to the model proposed here need to be developed. This requires careful electron back-scattered diffraction (EBSD) work in three dimensions and is the subject of a study about to begin.

Acknowledgements

We thank Paul for many years of discussions, his commitment to perfection has always inspired us. We thank Tom Blenkinsop and Jorn Kruhl for discussions concerning fractal geometries and measurement of their fractal dimension. Rob Twiss and Michael Stipp are thanked for critical and helpful reviews.

Appendix A. The deformation compatibility relation

We consider two domains labelled (+) and (−) in Fig. A1 separated by a surface Σ. $\boldsymbol{N}$ is the unit normal to the surface at P and we have selected coordinate systems x_i , y_i so that x_2 and y_2 are parallel to $\boldsymbol{N}$ and x_1, y_2 are tangent to Σ. Deformations defined by $\boldsymbol{y} = \boldsymbol{F}^{+}\boldsymbol{x} + \boldsymbol{c}$ and $\boldsymbol{y} = \boldsymbol{F}^{-}\boldsymbol{x} + \boldsymbol{c}$ occur in the two domains where $\boldsymbol{c}$ and $\boldsymbol{d}$ are constant displacement vectors. We are interested in the conditions under which the deformation $\boldsymbol{y}$ is continuous across Σ but the deformation gradients are discontinuous.

For compatibility between two domains characterised by two deformation gradients, $\boldsymbol{F}^{+}$ and $\boldsymbol{F}^{-}$, an arbitrary tangent to the boundary surface separating the two domains before deformation must be equally distorted and rotated by both $\boldsymbol{F}^{+}$ and $\boldsymbol{F}^{-}$ during the deformation. This is a way of saying that the boundary surface must be an invariant surface in both deformations. Hence, on the boundary

$$\boldsymbol{F}^{+}\boldsymbol{x} + \boldsymbol{c} = \boldsymbol{F}^{-}\boldsymbol{x} + \boldsymbol{d}$$

or,

$$\left(\boldsymbol{F}^{+} - \boldsymbol{F}^{-}\right)\boldsymbol{x} = \boldsymbol{d} - \boldsymbol{c}$$

For $\boldsymbol{y}$ to be continuous across the boundary $\boldsymbol{d} = \boldsymbol{c}$ and hence if $\boldsymbol{l}$ is a line in the boundary

$$\boldsymbol{F}^{+}\boldsymbol{l} = \boldsymbol{F}^{-}\boldsymbol{l}$$

which says that $\boldsymbol{F}^{+}$ deforms $\boldsymbol{l}$ in the same way that $\boldsymbol{F}^{-}$ does and hence Σ is an invariant surface in the bulk deformation.

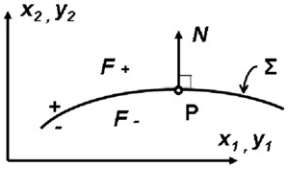

Fig. A1. A surface Σ with local normal $\boldsymbol{N}$ between two deformation gradients $\boldsymbol{F}^{+}$ and $\boldsymbol{F}^{-}$.

If $\boldsymbol{y}$ is continuous across the boundary then the following relations hold.

$(\partial y_1/\partial x_1)^+ = (\partial y_1/\partial x_1)^-$ and $(\partial y_2/\partial x_1)^+ = (\partial y_2/\partial x_1)^-$

There are no restrictions on $(\partial y_1/\partial x_2)^{\pm}$ or $(\partial y_2/\partial x_2)^{\pm}$. Hence $(\boldsymbol{F}^+ - \boldsymbol{F}^-)$ must be of the form

$$\left(\boldsymbol{F}^+ - \boldsymbol{F}^-\right) = \begin{bmatrix} 0 & \alpha \\ 0 & \beta \end{bmatrix}$$

where $\alpha = (\partial y_1/\partial x_2)^+ - (\partial y_1/\partial x_2)^-$ and $\beta = (\partial y_2/\partial x_2)^+ - (\partial y_2/\partial x_2)^-$. Thus $(\boldsymbol{F}^+ - \boldsymbol{F}^-)$ is a rank-1 matrix and hence can be expressed in the form

$$\left(\boldsymbol{F}^+ - \boldsymbol{F}^-\right) = \boldsymbol{a}\otimes\boldsymbol{b}$$

where $\boldsymbol{a}$ and $\boldsymbol{b}$ are vectors. This follows since the dyadic product of two vectors is always a rank-1 matrix. In particular since compatibility is required across the plane whose normal is $\boldsymbol{N}$ we can write

$$\left(\boldsymbol{F}^+ - \boldsymbol{F}^-\right) = \boldsymbol{a}\otimes\boldsymbol{N}$$

where $\boldsymbol{a}$ is an arbitrary vector. It follows that

$$\boldsymbol{F}^+\boldsymbol{l} - \boldsymbol{F}^-\boldsymbol{l} = (\boldsymbol{a}\otimes\boldsymbol{N})\boldsymbol{l} = \boldsymbol{a}(\boldsymbol{l}\cdot\boldsymbol{N}) = 0$$

since $\boldsymbol{l}$ is normal to $\boldsymbol{N}$. Hence

$$\boldsymbol{F}^+\boldsymbol{l} = \boldsymbol{F}^-\boldsymbol{l}.$$

which means that both $\boldsymbol{F}^+$ and $\boldsymbol{F}^-$ deform an arbitrary line $\boldsymbol{l}$ in the boundary equally. Hence the compatibility condition is

$$\boldsymbol{F}^+ - \boldsymbol{F}^- = \boldsymbol{a}\otimes\boldsymbol{N}$$

These same arguments apply in three dimensions. This relation is known as the Hadamard jump condition in the literature; it represents a discontinuity or jump in the deformation gradient but ensures continuity of the deformation across the boundary. Although resort to off axis Mohr circle constructions could be used to arrive at these conditions in two dimensions there is apparently no way of using such constructions for three dimensional deformations.

As an example consider the following example. A grain is divided into two domains A^+ and A^- by a boundary Σ with normal $\boldsymbol{N}$ as shown in Fig. A2. Coordinate axes x_i are chosen as shown.

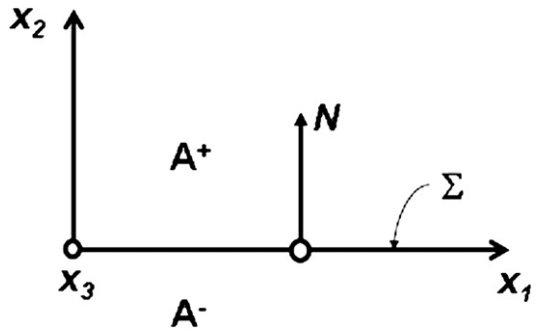

Fig. A2. A surface Σ with normal $\boldsymbol{N}$ between two domains A^+ and A^-.

The deformation gradients in A^+ and A^- are given by $\boldsymbol{F}^+ = \begin{bmatrix} 1 & \gamma & 0 \\ 0 & 1 & 0 \\ 0 & 0 & 1 \end{bmatrix}$ and $\boldsymbol{F}^- = \begin{bmatrix} 1 & -\gamma & 0 \\ 0 & 1 & 0 \\ 0 & 0 & 1 \end{bmatrix}$ so that $\boldsymbol{F}^+ - \boldsymbol{F}^- = \begin{bmatrix} 0 & 2\gamma & 0 \\ 0 & 0 & 0 \\ 0 & 0 & 0 \end{bmatrix} = 2\gamma \begin{bmatrix} 1 \\ 0 \\ 0 \end{bmatrix} \otimes \begin{bmatrix} 0 \\ 1 \\ 0 \end{bmatrix} = 2\gamma\boldsymbol{a}\otimes\boldsymbol{N}$ where $\boldsymbol{a}$ is a vector parallel to x_1. $\boldsymbol{F}^+ - \boldsymbol{F}^-$ is a rank-1 matrix and the grain undergoes a simple shear through the combined deformation in A^+ and A^-.

Appendix B. The deformation arising from single slip

As a simple example of the deformation gradient that arises from single slip we take the situation shown in Fig. B1(a) where $\boldsymbol{s}$ is the vector [1 0] and $\boldsymbol{m}$ is the vector [0 1]. Then $\gamma\boldsymbol{s}\otimes\boldsymbol{m} = \begin{bmatrix} 0 & \gamma \\ 0 & 0 \end{bmatrix}$ and $\boldsymbol{F} = \boldsymbol{I} + \gamma\boldsymbol{s}\otimes\boldsymbol{m} = \begin{bmatrix} 1 & \gamma \\ 0 & 1 \end{bmatrix}$. The deformation is given by $x_1 = X_1 + \gamma X_2$ and $x_2 = X_2$ so that the deformation is a simple shear with a shear of γ. Thus $\boldsymbol{F}^T\boldsymbol{F} = \begin{bmatrix} 1 & \gamma \\ \gamma & 1+\gamma^2 \end{bmatrix}$ and the deformation is isochoric since the determinant of $\boldsymbol{F}^T\boldsymbol{F}$ equals 1. The eigenvalues of $\boldsymbol{F}^T\boldsymbol{F}$ are $1/2\{(2+\gamma^2) \pm \gamma\sqrt{4+\gamma^2}\}$ and the rotation is anticlockwise through an angle $\tan^{-1}(\gamma/2)$. Thus if $\gamma = 1$ the principal stretches are 1.618 and 0.618 and the rotation is 26.57°. The total deformation, $\boldsymbol{F}$, is shown in Fig. A1(b) and comprises a plastic deformation, $\boldsymbol{U}^P$, with principal stretches given above and an anticlockwise lattice rotation, $\boldsymbol{R}^L$, through 26.57° such that $\boldsymbol{F} = \boldsymbol{R}^L\boldsymbol{U}^P$ which corresponds to Equation (3b).

Fig. B1. Deformation resulting from single slip (a) Undeformed state. (b) The deformed state with deformation gradient $\boldsymbol{F}$

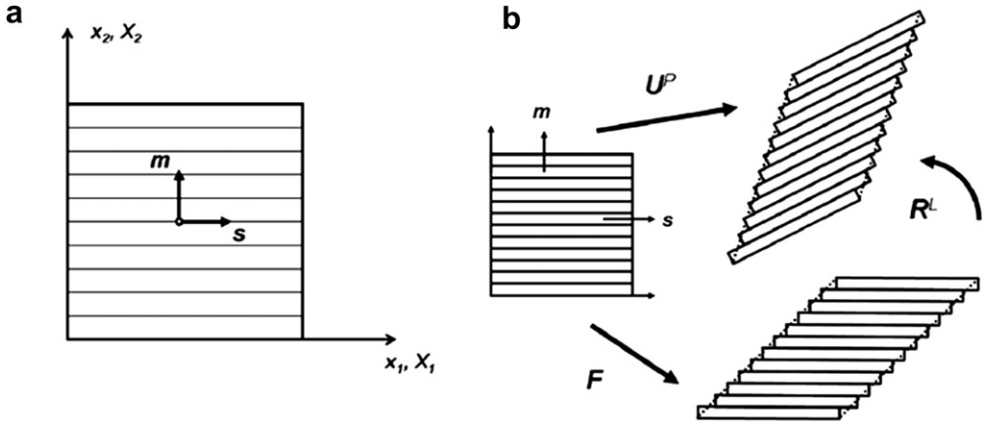

represented by a plastic stretch $\boldsymbol{U}^{\mathrm{P}}$ and a lattice rotation $\boldsymbol{R}^{\mathrm{L}}$.

In addition a general deformation may also involve an overall rigid rotation $\boldsymbol{R}$ so that the complete general deformation gradient that arises from single slip is $\boldsymbol{F} = \boldsymbol{R}(\mathbf{I} + \gamma \boldsymbol{s} \otimes \boldsymbol{m})$.

References

Ardell, A.J., Christie, J.M., McCormick, J.W., 1974. Dislocation images in quartz and the determination of Burgers vectors. The Philosophical Magazine 29, 1399–1411.

Asaro, R.J., 1983. Micromechanics of crystals and polycrystals. Advances in Applied Mechanics 23, 1–115.

Baeta, R.D., Ashbee, K.H.G., 1968. In: Bocciarelli, D.S. (Ed.), Evidence of plastic deformation of quartz at atmospheric pressure. Abstracts, Fourth European Regional Conference on Electron Microscopy, Rome, pp. 427–428.

Baeta, R.D., Ashbee, K.H.G., 1969a. Slip systems in quartz: I. experiments. The American Mineralogist 54, 1551–1573.

Baeta, R.D., Ashbee, K.H.G., 1969b. Slip systems in quartz: II. interpretation. The American Mineralogist 54, 1574–1582.

Ball, J.M., 1977. Convexity conditions and existence theorems in nonlinear elasticity. Archive for Rational Mechanics and Analysis 63, 337–403.

Ball, J.M., 2004. Mathematical models of martensitic microstructure. Materials Science and Engineering A 378, 61–69.

Ball, J.M., James, R.D., 1987. Fine phase mixtures as minimizers of energy. Archive for Rational Mechanics and Analysis 100, 13–52.

Bestmann, M., Prior, D.J., 2003. Intragranular dynamic recrystallization in naturally deformed calcite marble: diffusion accommodated grain boundary sliding as a result of subgrain rotation recrystallization. Journal of Structural Geology 25, 1597–1613.

Bhattacharya, K., 2003. Microstructure of Martensite: Why It Forms and How It Gives Rise to the Shape-memory Effect. Oxford University Press, 288 pp.

Biot, M.A., 1955. Variational principles in irreversible thermodynamics with application to viscoelasticity. The Physical Review 97, 1463–1469.

Biot, M.A., 1958. Linear thermodynamics and the mechanics of solids. In: Proceedings Third U.S. National Congress of Applied Mechanics, Brown University, Providence, R.I. ASME, New York, pp. 1–18.

Bishop, J.F.W., Hill, R., 1951. A theory of the plastic distortion of a polycrystalline aggregate under combined stresses. Philosophical Magazine 42, 414–427.

Bouchez, J.L., 1978. Preferred orientations of quartz (a) axes in some tectonites - kinematic inferences. Tectonophysics 49, T25–T30.

Bouchez, J.L., Lister, G.S., Nicolas, A., 1983. Fabric asymmetry and shear sense in movement zones. Geologische Rundschau 72, 401–419.

Brodie, K., Rutter, E., 1987. The role of transiently fine-grained reaction products in syntectonic metamorphism: natural and experimental examples. Canadian Journal of Earth Sciences 24, 556–564.

Bronkhorst, C.A., Kalidindi, S.R., Anand, L., 1992. Polycrystalline plasticity and the evolution of crystallographic texture in FCC metals. Philosophical Transactions: Physical Sciences and Engineering 341, 443–477.

Cahn, J.W., Larche, F., 1984. A simple model for coherent equilibrium. Acta Materialia 32, 1915–1923.

Carstensen, C., Hackl, K., Mielke, A., 2002. Non-convex potentials and microstructures in finite-strain plasticity. Proceedings of the Royal Society London A 458, 299–317.

Choksi, R., Del Piero, G., Fonseca, I., Owen, D., 1999. Structured deformations as energy minimizers in models of fracture and hysteresis. Mathematics and Mechanics of Solids 4, 321–356.

Christie, J.M., Griggs, D.T., Carter, N.L., 1964. Experimental evidence of basal slip in quartz. The Journal Of Geology 72, 734–756.

Cobbold, P.R., Gapais, D., 1986. Slip-system domains. I. Plane-strain kinematics of arrays of coherent bands with twinned fibre orientations. Tectonophysics 137, 113–132.

Cross, M.C., Hohenberg, P.C., 1993. Pattern formation outside of equilibrium. Reviews of Modern Physics 65, 851–1112.

de Ronde, A.A., Heilbronner, R., Stunitz, H., Tullis, J., 2004. Spatial correlation of deformation and mineral reaction in experimentally deformed plagioclase-olivine aggregates. Tectonophysics 389, 93–109.

De Wit, A., Borckmans, P., Dewel, G., 1997. Twist grain boundaries in three-dimensional lamellar Turing structures. Proceedings of the National Academy of Sciences USA 94, 12765–12768.

Del Piero, G., Truskinovsky, L., 2001. Macro- and micro-cracking in one-dimensional elasticity. International Journal of Solids and Structures 38, 1135–1148.

Dell'Angelo, L.N., Tullis, J., 1989. Fabric development in experimentally sheared quartzites. Tectonophysics 169, 1–21.

Delle Piane, C., Burlini, L., Grobety, B., 2007. Reaction-induced strain localization: torsion experiments on dolomite. Earth and Planetary Science Letters 256, 36–46.

Delle Piane, C., Wilson, C.J.L., Burlini, L., 2009. Dilatant plasticity in high-strain experiments on calcite–muscovite aggregates. Journal of Structural Geology 31, 1084–1099.

Dillamore, I.L., Roberts, J.G., Bush, A.C., 1979. Occurrence of shear bands in heavily rolled cubic metals. Metal Science 13, 73–77.

Dmitrieva, O., Dondl, P.W., Muller, S., Raabe, D., 2009. Lamination microstructure in shear deformed copper single crystals. Acta Materialia 57, 3439–3449.

Drury, M.R., Humphreys, F.J., White, S.H., 1985. Large strain deformation studies using polycrystalline magnesium as a rock analog. 2. Dynamic recrystallization mechanisms at high-temperatures. Physics of the Earth and Planetary Interiors 40, 208–222.

Epstein, I.R., Pojman, J.A., 1998. An Introduction to Nonlinear Chemical Dynamics. Oxford University Press, New York, 392 pp.

Ericksen, J.L., 1975. Equilibrium of bars. Journal of Elasticity 5, 191–202.

Ericksen, J.L., 1998. Introduction to the Thermodynamics of Solids. Springer, New York, 189 pp.

Eshelby, J.D., 1975. The elastic energy-momentum tensor. Journal of Elasticity 5, 321–335.

Etchecopar, A., 1977. A plane kinematic model of progressive deformation in a polycrystalline aggregate. Tectonophysics 39, 121–139.

Etchecopar, A., Vasseur, G., 1987. A 3D kinematic model of fabric development in polycrystalline aggregates: comparisons with experimental and natural samples. Journal of Structural Geology 9, 705–717.

Fairbairn, H.W., 1949. Structural Petrology of Deformed Rocks. Addison-Wesley, Cambridge, Mass, 344 pp.

Francfort, G.A., Marigo, J.-J., 1998. Revisiting brittle fracture as an energy minimization problem. Journal of the Mechanics and Physics of Solids 46, 1319–1342.

Gapais, D., Cobbold, P.R., 1987. Slip system domains. 2. Kinematic aspects of fabric development in polycrystalline aggregates. Tectonophysics 138, 289–309.

Garcia Celma, A., 1982. Domainal and fabric heterogeneities in the Cap de Creus quartz mylonites. Journal of Structural Geology 4, 443–455.

Gibbs, J.W., 1906. Collected Works of J. Willard Gibbs, vol. 1. Yale University Press, New Haven, 434 pp.

Glimm, T., Hentschel, H.G.E., 2008. On isoconcentration surfaces of three dimensional Turing patterns. The International Journal of Bifurcation and Chaos 18, 391–406.

Groves, G.W., Kelly, A., 1969. Change of shape due to dislocation climb. Philosophical Magazine 19, 977–986.

Guillope, M., Poirier, J.P., 1979. Dynamic recrystallisation during creep of single-crystalline halite - experimental study. Journal of Geophysical Research 84, 5557–5567.

Hähner, P., Bay, K., Zaiser, M., 1998. Fractal dislocation patterning during plastic deformation. Physical Review Letters 81, 2470–2473.

Halfpenny, A., Prior, D., Wheeler, J., 2006. Analysis of dynamic recrystallization and nucleation in a quartzite mylonite. Tectonophysics 427, 3–14.

Hansen, B.L., Bronkhorst, C.A., Ortiz, M., 2010. Dislocation subgrain structures and modeling the plastic hardening of metallic single crystals. Modelling and Simulation in Materials Science and Engineering 18 055001.

Havner, K.S., 2005. On lattice and material-frame rotations and crystal hardening in high-symmetry axial loading. Philosophical Magazine 85, 2861–2894.

Heilbronner, R., Tullis, J., 2006. Evolution of c axis pole figures and grain size during dynamic recrystallization: results from experimentally sheared quartzite. Journal of Geophysical Research 111 (B10202).

Hirth, G., Tullis, J., 1992. Dislocation creep regimes in quartz aggregates. Journal of Structural Geology 14, 145–159.

Hobbs, B.E., 1966. Microfabrics of tectonites from the Wyangala Dam area, New South Wales, Australia. Geological Society of America Bulletin 77, 685–706.

Hobbs, B.E., 1968. Recrystallisation of single crystals of quartz. Tectonophysics 6, 353–401.

Hobbs, B.E., Ord, A., 2010. The development of microstructure within deforming-reactive systems. Geological Society of London, in press.

Hobbs, B.E., Ord, A., Spalla, I., Gosso, G., Zucalli, M., 2010. The interaction of deformation and metamorphic reactions. In: Geological Society of London, Special Issue, vol. 332, pp. 189–223.

Hobbs, B.E., Ord, A., Regenauer-Lieb, K. The continuum thermodynamics of deformed metamorphic rocks: a review. Journal of Structural Geology, in press.

Houlsby, G.T., Puzrin, A.M., 1999. An approach to plasticity based on generalised thermodynamics. Proc. Int. Symp. Hypoelasticity, Horton, Greece, pp. 233–245.

Houlsby, G.T., Puzrin, A.M., 2006. Principles of Hyperplasticity. Springer-Verlag, London, 351 pp.

Hull, D., 1999. Fractography. Cambridge University Press, 366 pp.

Hunt, B.W., Peletier, M.A., Wadee, M.A., 2001. The Maxwell stability criterion in pseudo-energy models of kink banding. Journal of Structural Geology 22, 669–681.

Jeřábek, P., Stünitz, H., Heilbronner, R., Lexa, O., Schulmann, K., 2007. Microstructural-deformation record of an orogen-parallel extension in the Vepor Unit, West Carpathians. Journal of Structural Geology 29, 1722–1743.

Jessell, M.W., Lister, G.S., 1990. A simulation of the temperature-dependence of quartz fabrics. Deformation Mechanisms, Rheology and Tectonics 54, 353–362.

Jiang, Z.T., Prior, D.J., Wheeler, J., 2000. Albite crystallographic preferred orientation and grain misorientation distribution in a low-grade mylonite: implications for granular flow. Journal of Structural Geology 22, 1663–1674.

Kagan, Y.Y., 2007. Earthquake spatial distribution: the correlation dimension. Geophysical Journal International 168, 1175–1194.

Kocks, U.F., 1960. Polyslip in single crystals. Acta Metallurgica 8, 345–352.

Kocks, U.F., Tome, C.N., Wenk, H.-R., 1998. Texture and Anisotropy. Cambridge University Press, Cambridge.

Koenig, E., Chainais, P., 2008. Multifractal analysis on the sphere. In: Elmoataz, A., et al. (Eds.), ICISP 2008, LNCS 5099. Springer-Verlag, Berlin, pp. 613–621.

Kohn, K.V., 1991. The relaxation of a double-well energy. Continuum Mechanics and Thermodynamics 3, 193–236.

Kondepudi, D., Prigogine, I., 1998. Modern Thermodynamics. John Wiley, Chichester, 486 pp.
Kruhl, J.H., Nega, M., 1996. The fractal shape of sutured quartz boundaries: application as a geothermometer. Geologische Rundschau 85, 34–43.
Law, R.D., Searle, M.P., Simpson, R.L., 2004. Strain, deformation temperatures and vorticity of flow at the top of the Greater Himalayan Slab, Everest Massif, Tibet. In: Journal of the Geological Society, London, vol. 161, pp. 305–320.
Linker, M.F., Kirby, S.H., Ord, A., Christie, J.M., 1984. Effects of compression direction on the plasticity and rheology of hydrolytically weakened synthetic quartz crystals at atmospheric pressure. Journal of Geophysical Research 89, 4241–4255.
Lister, G.S., Hobbs, B.E., 1980. The simulation of fabric development during plastic deformation and its application to quartzite: the influence of deformation history. Journal of Structural Geology 2, 355–370.
Lister, G.S., Paterson, M.S., Hobbs, B.E., 1978. The simulation of fabric development in plastic deformation and its application to quartzite: the model. Tectonophysics 45, 107–158.
Lloyd, G.E., Law, R.D., Mainprice, D., 2010. Predicting seismic properties from three-dimensional microstructures - a new look at an old quartzite. In: Geological Society, London, Special Publications, vol. 335, pp. 603–622.
Lyakhovsky, V., Ben-Zion, Y., Agnon, A., 1997. Distributed damage, faulting and friction. Journal of Geophysical Research 102, 27635–27649.
Lyakhovsky, V., Ben-Zion, Y., 2008. Scaling relations of earthquakes, aseismic deformation and evolving fault structures in a damage rheology model. Geophysical Journal International 172, 651–662.
Lyakhovsky, V., Hamiel, Y., Ben-Zion, Y. A nonlocal visco-elastic damage model and dynamic fracturing. Journal of the Mechanics and Physics of Solids, submitted for publication.
Mamtani, M.A., 2010. Strain-rate estimation using fractal analysis of quartz grains in naturally deformed rocks. Journal Geological Society of India 75, 202–209.
Mamtani, M.A., Greiling, R.O., 2010. Serrated quartz grain boundaries, temperature and strain rate: Testing fractal techniques in a syntectonic granite. In: Spalla, M.I., Marotta, A.M., Gosso, G. (Eds.), Advances in Interpretation of Geological Processes: Refinement of Multi-scale Data and Integration in Numerical Modelling. Geological Society, London, Special Publications, vol. 332, pp. 35–48.
Mancktelow, N., 2004. The influence of grain boundary fluids on the microstructure of quartz-feldspar mylonites. Journal of Structural Geology 26, 47–69.
Mandelbrot, B.B., 1983. The Fractal Geometry of Nature. Freeman, New York, 468 pp.
Mangasarian, O.L., 1994. Non-linear Programming. Classics in Applied Mathematics. Society for Industrial and applied Mathematics, Philadelphia, 220 pp.
Marsden, J.E., Hughes, T.J.R., 1983. Mathematical Foundations of Elasticity. Prentice-Hall, New Jersey, 556 pp.
McLaren, A.C., Turner, R.G., Boland, J.N., Hobbs, B.E., 1970. Dislocation structure of the deformation lamellae in synthetic quartz; a study by electron and optical microscopy. Contributions to Mineralogy and Petrology 29, 104–115.
Means, W.D., 1983. Application of the Mohr-circle construction to problems of in homogeneous deformation. Journal of Structural Geology 5, 279–286.
Menegon, L., Pennacchioni, G., Heilbronner, R., Pittarello, L., 2008. Evolution of quartz microstructure and c-axis crystallographic preferred orientation within ductilely deformed granitoids (Arolla unit, Western Alps). Journal of Structural Geology 30, 1332–1347.
Miehe, C., Schotte, J., Lambrecht, M., 2002. Homogenisation of inelastic solid materials at finite strains based on incremental minimisation principles: application to the texture analysis of polycrystals. Journal of the Mechanics and Physics of Solids 50, 2123–2167.
Miehe, C., Lambrecht, M., Gurses, E., 2004. Analysis of material instabilities in inelastic solids by incremental energy minimisation and relaxation methods: evolving deformation microstructures in finite plasticity. Journal of the Mechanics and Physics of Solids 52, 2725–2769.
Morrison-Smith, D.J., Paterson, M.S., Hobbs, B.E., 1976. An electron microscope study of plastic deformation in single crystals of synthetic quartz. Tectonophysics 33, 43–79.
Murdzek, R., 2007. The box-counting method in the large scale structure of the universe. Romanian Journal of Physics 52, 149–154.
Nadai, A., 1950. Theory of Flow and Fracture of Solids. McGraw-Hill, New York, 572 pp.
Nye, J.F., 1957. Physical Properties of Crystals. Clarendon Press, Oxford, 322 pp.
Oertel, G., 1983. Construction of crossed girdles by superposing four subfabrics, each with a single maximum. Geologische Rundschau 72, 451–467.
Oertel, G.F., 1996. Stress and Deformation: a Handbook on Tensors in Geology. Oxford University Press, 292 pp.
Ord, A., Kirby, S.H., 1982. Burgers vectors in deformed synthetic quartz. Australian Conference in Electron Microscopy and Cell Biology Abstracts, Canberra.
Ortiz, M., 1999. Plastic yielding as a phase transition. Journal of Applied Mechanics 66, 289–298.
Ortiz, M., Repetto, E.A., 1999. Nonconvex energy minimization and dislocation structures in ductile single crystals. Journal of the Mechanics and Physics of Solids 47, 397–462.
Ortiz, M., Repetto, E.A., Stainier, L., 2000. A theory of subgrain dislocation structures. Journal of the Mechanics and Physics of Solids 48, 2077–2114.
Ortoleva, P.J., 1989. Nonequilibrium reaction-diffusion structures in rigid and visco-elastic media: knots and unstable noninertial flows. Modelisation mathematique et analyse numerique 23, 507–517.
Ortoleva, P.J., Ross, J., 1974. On a variety of wave phenomena in chemical reactions. Journal of Chemical Physics 59, 5090–5107.
Ortoleva, P.J., Merino, E., Strickholm, P., 1982. Kinetics of metamorphic layering in anisotropically stressed rock. American Journal of Science 282, 617–643.
Paterson, M.S., 1969. The ductility of rocks. In: Argon, A.S. (Ed.), Physics of Strength and Plasticity. The Orowan 65th Anniversary Volume. M.I.T. Press, pp. 377–392.
Pauli, C., Schmid, S.M., Heilbronner, R.P., 1996. Fabric domains in quartz mylonites: localised three dimensional analysis of microstructure and texture. Journal of Structural Geology 18, 1183–1203.
Piercy, G.R., Cahn, R.W., Cottrell, A.H., 1955. A study of primary and conjugate slip in crystals of alpha brass. Acta Metallurgica 3, 331–338.
Pipkin, A.C., 1993. Convexity conditions for strain-dependent energy functions for membranes. Archive for Rational Mechanics and Analysis 121, 361–376.
Poirier, J.P., Nicolas, A., 1975. Deformation-induced recrystallization due to progressive misorientation of subgrains, with special reference to mantle peridotites. Journal of Geology 83, 707–720.
Rice, J., 1971. Inelastic constitutive relations for solids: an internal-variable theory and its application to metal plasticity. Journal of the Mechanics and Physics of Solids 19, 433–455.
Rice, J., 1975. Continuum mechanics and thermodynamics of plasticity in relation to microscale deformation mechanisms. In: Argon, A.S. (Ed.), Constitutive Equations in Plasticity. MIT Press, Cambridge, Mass, pp. 23–79.
Rubie, D.C., 1983. Reaction-enhanced ductility; the role of solid-solid univariant reactions in deformation of the crust and mantle. Tectonophysics 96, 331–352.
Sander, B., 1911. Uber Zusammenhange zwischen Teilbewegung und Gefuge in Gesteinen. Tschermaks mineralogische und petrographische Mitteilungen 30, 281–314.
Sander, B., 1930. Gefügekunde der Gesteine mit besonderer Berücksichtingung der Tektonite. Springer, Vienna.
Sander, B., 1970. An Introduction to the Study of Fabrics of Geological Bodies. Pergamon Press, Oxford (translation by Phillips, F.C., & Windsor, G. of Einführung in die Gefügekunde der geologischen Körper, 1948–1950, Vienna).
Schmid, S.M., 1994. Textures of geological materials: computer model predictions versus empirical interpretations based on rock deformation experiments and field studies. In: Bunge, H.J., et al. (Eds.), Textures of Geological Materials. DGM Informationsges, Uberursel, Germany, pp. 279–301.
Schmid, S.M., Casey, M., 1986. Complete fabric analysis of some commonly observed quartz c-axis patterns. In: Hobbs, B.E., Heard, H.C. (Eds.), Mineral and Rock Deformation: Laboratory Studies. The Paterson Volume. Geophysical Monograph, vol. 36. American Geophysical Union, pp. 263–286.
Schmid, S.M., Paterson, M.S., Boland, J.N., 1980. High temperature flow and dynamic recrystallization in Carrara marble. Tectonophysics 65, 245–280.
Silhavy, M., 1991. Rank 1 perturbations of deformation gradients. International Journal of Solids and Structures 38, 943–965.
Silhavy, M., 1997. The Mechanics and Thermodynamics of Continuous Media. Springer, Berlin, 504 pp.
Stipp, M., Kunze, K., 2008. Dynamic recrystallization near the brittle-plastic transition in naturally and experimentally deformed quartz aggregates. Tectonophysics 448, 77–97.
Stipp, M., Stunitz, H., Heilbronner, R., Schmid, S.M., 2002. The eastern Tonale fault zone: a 'natural laboratory' for crystal plastic deformation of quartz over a temperature range from 250 to 700 degrees C. Journal of Structural Geology 24, 1861–1884.
Stipp, M., Tullis, J., Scherwath, M., Behrmann, J.H., 2010. A new perspective on paleopiezometry: dynamically recrystallized grain size distributions indicate mechanism changes. Geology 38, 759–762.
Streitenberger, P., Forster, D., Kolbe, G., Veit, P., 1995. The fractal geometry of grain boundaries in deformed and recovered zinc. Scripta Metallurgica et Materialia 33, 546.
Stunitz, H., Tullis, J., 2001. Weakening and strain localization produced by syn-deformational reaction of plagioclase. International Journal of Earth Sciences 90, 136–148.
Takahashi, M., Nagahama, H., Masuda, T., Fujimura, A., 1998. Fractal analysis of experimentally, dynamically recrystallized quartz grains and its possible application as a strain-rate meter. Journal of Structural Geology 20, 269–275.
Taylor, G.I., 1938. Plastic strains in metals. Journal Institute of Metals 62, 307–324.
Tome, C.N., Lebensohn, R.A., Necker, C.T., 2002. Mechanical anisotropy and grain interaction in recrystallized aluminum. Metallurgical and Materials Transactions A 33A, 2635–2648.
Trepied, L., Doukhan, J.-C., 1982. Evidence of $\bar{a}\langle\bar{a}+\overline{c}\rangle$ dislocations in synthetic quartz crystals compressed along the $\overline{c}$ axis. Bulletin de Mineralogie 105, 176–180.
Trepied, L., Doukhan, J.C., Paquet, J., 1980. Subgrain boundaries in quartz. Theoretical analysis and microscopic observations. Physics and Chemistry of Minerals 5, 201–218.
Truskinovsky, L., Zanzotto, G., 1996. Ericksen's bar revisited: energy wiggles. Journal of the Mechanics and Physics of Solids 44, 1371–1408.
Tungatt, P.D., Humphreys, F.J., 1981. An in-situ optical investigation of the deformation behaviour of sodium nitrate - an analogue for calcite. Tectonophysics 78, 661–675.
Turner, F.J., Weiss, L.E., 1963. Structural Analysis of Metamorphic Tectonites. McGraw Hill, New York, 545 pp.
Twiss, R.J., 1974. Structure and significance of planar deformation features in synthetic quartz. Geology 2, 329–332.
Twiss, R.J., 1976. Some planar deformation features, slip systems, and submicroscopic structures in synthetic quartz. The Journal of Geology 84, 701–772.

van Daalen, M., Heilbronner, R., Kunze, K., 1999. Orientation analysis of localized shear deformation in quartz fibres at the brittle-ductile transition. Tectonophysics 303, 83–107.
Vernon, R.H., 2004. A Practical Guide to Rock Microstructure. Cambridge University Press, Cambridge, 594 pp.
Wenk, H.-R., 1999. A voyage through the deformed Earth with the self-consistent model. Modelling and Simulation in Materials Science and Engineering 7, 699–722.
White, S., 1973. The dislocation structures responsible for the optical effects in some naturally- deformed quartzes. Journal of Materials Science 8, 490–499.
White, S., 1977. Geological significance of recovery and recrystallization processes in quartz. Tectonophysics 39, 143–170.
Wintsch, R.P., 1985. The possible effects of deformation on chemical processes in metamorphic fault zones. chap. 10. In: Thompson, A.B. (Ed.), Metamorphic Reactions: Kinetics, Textures and Deformation. Advances in Physical Geochemistry, vol. 4, pp. 251–268.
Zhang, G., Hynes, A., 1995. Determination of position-gradient tensor from strain measurements and its implications for the displacement across a shear zone. Journal of Structural Geology 17, 1587–1599.